ARTICLE

TDP-43 and RNA form amyloid-like myo-granules in regenerating muscle

Thomas O. Vogler[1,2,15], Joshua R. Wheeler[2,3,15], Eric D. Nguyen[2,4], Michael P. Hughes[5,6], Kyla A. Britson[7,8], Evan Lester[2,3], Bhalchandra Rao[3], Nicole Dalla Betta[1], Oscar N. Whitney[1], Theodore E. Ewachiw[1], Edward Gomes[9], James Shorter[9], Thomas E. Lloyd[7,8], David S. Eisenberg[5,6,10], J. Paul Taylor[11,12], Aaron M. Johnson[4,13], Bradley B. Olwin[1]* & Roy Parker[3,14]*

A dominant histopathological feature in neuromuscular diseases, including amyotrophic lateral sclerosis and inclusion body myopathy, is cytoplasmic aggregation of the RNA-binding protein TDP-43. Although rare mutations in *TARDBP*—the gene that encodes TDP-43—that lead to protein misfolding often cause protein aggregation, most patients do not have any mutations in *TARDBP*. Therefore, aggregates of wild-type TDP-43 arise in most patients by an unknown mechanism. Here we show that TDP-43 is an essential protein for normal skeletal muscle formation that unexpectedly forms cytoplasmic, amyloid-like oligomeric assemblies, which we call myo-granules, during regeneration of skeletal muscle in mice and humans. Myo-granules bind to mRNAs that encode sarcomeric proteins and are cleared as myofibres mature. Although myo-granules occur during normal skeletal-muscle regeneration, myo-granules can seed TDP-43 amyloid fibrils in vitro and are increased in a mouse model of inclusion body myopathy. Therefore, increased assembly or decreased clearance of functionally normal myo-granules could be the source of cytoplasmic TDP-43 aggregates that commonly occur in neuromuscular disease.

The function and aggregation of the RNA-binding protein TAR DNA-binding protein 43 (TDP-43) in multinucleated skeletal-muscle cells (myofibres) is of interest for two reasons. First, TDP-43 aggregates accumulate in the skeletal muscle of patients with inclusion body myopathy, oculopharyngeal muscular dystrophy and distal myopathies[1,2]. These aggregates appear to be similar to the cytoplasmic TDP-43 aggregates that are found in the neurons of patients with amyotrophic lateral sclerosis and frontotemporal lobar degeneration, suggesting that there is a common mechanism in muscle and neurons that leads to histopathological, cytoplasmic TDP-43 aggregation[2–4]. Second, reducing the levels of TDP-43 leads to age-related muscle weakness in mice[5], muscle degeneration and sarcomere disruption in zebrafish[6] and age-related muscle weakness in *Drosophila* wing muscles[7,8]. Given the requirement for TDP-43 in muscle function and its potential to form cytoplasmic aggregates in muscle diseases, we examined TDP-43 function during normal mammalian skeletal-muscle formation.

Cytoplasmic TDP-43 myo-granules

We first examined the subcellular distribution of TDP-43 in cultured skeletal-muscle cells and found abundant nuclear TDP-43 in C2C12 myoblasts, a mouse muscle cell line[9] (Extended Data Fig. 1a). However, during the differentiation of C2C12 myoblasts and isolated primary mouse myoblasts into multinucleated myotubes, we observed an increase in cytoplasmic TDP-43 by immunofluorescence and by subcellular fractionation (Extended Data Fig. 1a–e). Furthermore, live-cell single-molecule imaging of HaloTag–TDP-43 revealed increased cytosolic HaloTag–TDP-43 in differentiating myotubes compared to myoblasts (Extended Data Fig. 1f–k and Supplementary Videos 1, 2).

We next examined the subcellular distribution of TDP-43 in uninjured tibialis anterior muscle and tibialis anterior muscle that was chemically injured using barium chloride ($BaCl_2$) and was subsequently allowed to regenerate[10,11] (Fig. 1a). Although we primarily observed nuclear TDP-43 in uninjured muscle, at five days post-injury (DPI) TDP-43 was upregulated and was found to be expressed in both the myonuclei and cytoplasm of newly forming myofibres, identified by embryonic myosin heavy chain (eMHC) expression (Fig. 1b and Extended Data Fig. 2a). Super-resolution microscopy revealed that TDP-43 was predominately localized to myonuclei in uninjured myofibres, whereas in regenerating myofibres cytoplasmic TDP-43 localized to regions surrounding eMHC (Fig. 1c), which are sites of newly formed sarcomeres[12]. By 10 DPI, cytosolic TDP-43 levels decreased and TDP-43 localized around the centrally located nuclei, whereas by 30 DPI, TDP-43 had relocalized to the nucleus (Fig. 1b, d and Extended Data Fig. 2b). Therefore, cytosolic TDP-43 increases during skeletal-muscle-cell formation in culture and in mice.

Because cytoplasmic TDP-43 localization is associated with pathological aggregation, we investigated whether the cytoplasmic TDP-43 identified in skeletal-muscle formation adopts a higher-order, oligomeric state. We detected an increase in urea-insoluble TDP-43 in myotubes compared to myoblasts and observed higher molecular weight SDS-resistant TDP-43 assemblies unique to differentiating myotubes by semi-denaturing detergent agarose-gel electrophoresis (Extended Data Fig. 2c, d). Furthermore, immunoprecipitation of TDP-43 from myotubes and from mouse tibialis anterior muscles at 5 DPI, followed by transmission electron microscopy (TEM), reveals the

[1]Department of Molecular, Cellular and Developmental Biology, University of Colorado, Boulder, CO, USA. [2]Medical Scientist Training Program, University of Colorado Anschutz Medical Campus, Aurora, CO, USA. [3]Department of Chemistry and Biochemistry, University of Colorado, Boulder, CO, USA. [4]Molecular Biology Program, Department of Biochemistry and Molecular Genetics, University of Colorado Anschutz Medical Campus, Aurora, CO, USA. [5]Department of Biological Chemistry, University of California, Los Angeles (UCLA), Los Angeles, CA, USA. [6]Department of Chemistry and Biochemistry, University of California, Los Angeles (UCLA), Los Angeles, CA, USA. [7]Departments of Neurology, Johns Hopkins University School of Medicine, Baltimore, MD, USA. [8]Departments of Neuroscience, Johns Hopkins University School of Medicine, Baltimore, MD, USA. [9]Department of Biochemistry and Biophysics, Perelman School of Medicine, University of Pennsylvania, Philadelphia, PA, USA. [10]Howard Hughes Medical Institute, University of California, Los Angeles (UCLA), Los Angeles, CA, USA. [11]Department of Cell and Molecular Biology, St. Jude Children's Research Hospital, Memphis, TN, USA. [12]Howard Hughes Medical Institute, St. Jude Children's Research Hospital, Memphis, TN, USA. [13]University of Colorado School of Medicine RNA Bioscience Initiative, University of Colorado Anschutz Medical Campus, Aurora, CO, USA. [14]Howard Hughes Medical Institute, University of Colorado, Boulder, CO, USA. [15]These authors contributed equally: Thomas O. Vogler, Joshua R. Wheeler. *e-mail: olwin@colorado.edu; roy.parker@colorado.edu
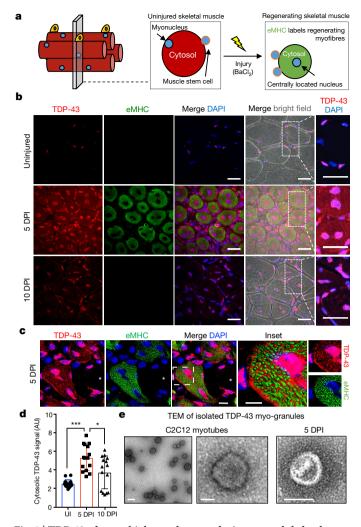
Fig. 1 | TDP-43 adopts a higher-order state during normal skeletal-muscle formation. a, Schematic of regeneration of skeletal muscle injuries in wild-type mice. **b**, TDP-43 expression after $BaCl_2$-induced tibialis anterior muscle injury. eMHC expression in regenerating myofibres; nuclei were counterstained with 4′,6-diamidino-2-phenylindole (DAPI). Scale bars, 25 μm. $n = 5$ mice per condition, each showing similar results. **c**, Super-resolution imaging of TDP-43 expression around nascent sarcomeres in the cytoplasm during muscle regeneration. Scale bar, 10 μm and 5 μm (inset). Asterisk, an uninjured myofibre that lacks eMHC and TDP-43 cytosolic signals. Nuclei are counterstained with DAPI. $n = 3$ biologically independent experiments, each showing similar results. **d**, Quantification of the cytoplasmic TDP-43 signal in skeletal muscle myofibres. AU, arbitrary units. Unpaired, two-tailed Student's t-tests were used for each individual comparison: 5 DPI versus uninjured (UI), ***$P = 4.36 \times 10^{-8}$; 5 DPI versus 10 DPI, *$P = 0.011$; 10 DPI versus UI, $P = 0.015$. $n = 3$ biological replicates, $n = 5$ myofibres per replicate. Data are mean ± s.d. **e**, TEM images of myo-granules isolated by TDP-43 immunoprecipitation obtained from C2C12 myotubes and from mouse tibialis anterior muscle at 5 DPI. $n = 3$ biologically independent experiments, each showing similar results.

presence of 50–250-nm assemblies that are not detected in undifferentiated myoblasts or in uninjured skeletal muscle (Fig. 1e and Extended Data Fig. 2e, f). The TEM structure is similar to previously characterized TDP-43 oligomers, albeit roughly twofold larger in diameter[13]. To exclude the possibility that the TDP-43 assemblies in skeletal muscle are stress granules, we assayed C2C12 myotubes for the stress granule markers G3BP1 and PABP1. Stress granules were not present during normal myotube formation (Extended Data Fig. 2g). Therefore, during muscle formation, TDP-43 exists as a component of an SDS-resistant oligomeric assembly that is distinct from stress granules and that we refer to as myo-granules.
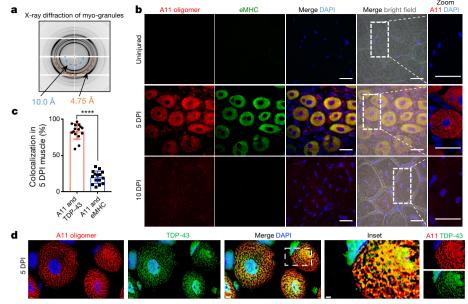
Myo-granules are amyloid-like assemblies

The SDS resistance of these myo-granules suggests that myo-granules have amyloid-like properties, which is supported by two observations. First, X-ray diffraction of lyophilized myo-granules revealed a diffraction pattern with a 4.8 Å reflection, indicating a β-rich complex that is not observed in control samples. Myo-granules lacked a 10 Å reflection, which suggests a lack of mated cross β-sheets similar to previously described amyloid-like oligomers[14] (Fig. 2a and Extended Data Fig. 3a, b). Second, immunopurified myo-granules from C2C12 myotubes and regenerating mouse tibialis anterior muscle also show A11 immunoreactivity, a conformation-specific antibody that recognizes β-rich structures, including amyloid-like oligomers[15] (Extended Data Fig. 3c–h).

Similar to TDP-43, A11 immunoreactivity increases in myotubes in culture and in regenerating mouse tibialis anterior muscle (Extended Data Fig. 3i–k). In developing myotubes in culture, A11 immunoreactivity is cytoplasmic and correlates with cytoplasmic TDP-43 expression (Extended Data Fig. 4a–c). During muscle regeneration A11 immunoreactivity correlates with TDP-43 cytoplasmic expression, increasing in the cytoplasm at 5 DPI but disappearing by 10 DPI (Fig. 2b and Extended Data Fig. 4d–g). At 5 DPI in mice, more than 80% of A11 immunoreactivity is co-localized with cytosolic TDP-43 expression (Fig. 2c, d and Extended Data Fig. 4h). Furthermore, cytoplasmic TDP-43 exists as a component of an A11-reactive complex, as revealed by proximity ligation assays in differentiating C2C12 myotubes (Extended Data Fig. 4i). These observations indicate that cytoplasmic myo-granules contain TDP-43 in an amyloid-like oligomer conformation during skeletal muscle formation.

Myo-granules contain sarcomeric mRNAs

Because TDP-43 is an RNA-binding protein, we examined whether myo-granules included RNA. Immunoprecipitation of myo-granules with TDP-43 or A11 antibodies followed by oligo-dT northern blot analysis reveals that TDP-43 and A11 associate with mRNA in myotubes (Extended Data Fig. 5a). To identify the mRNAs that are bound by TDP-43 during muscle formation, we constructed transcriptome-wide maps of TDP-43-binding sites in undifferentiated myoblasts and in myotubes using enhanced ultraviolet-light crosslinking and immunoprecipitation (eCLIP)[16] (Extended Data Fig. 5b–e). We identified a total of 556 binding sites across 174 genes for myoblasts and a total of 975 binding sites across 320 genes for myotubes that were significantly enriched compared to size-matched input (which reflects all RNA–protein interactions in the input). The binding sites were highly correlated between biological replicates, showed enrichment for the TDP-43 UG-rich consensus sequence and had thousands of reproducible CLIP clusters as shown by irreproducible discovery rate analysis; we identified known TDP-43 mRNA targets including the 3′ untranslated region of TDP-43[17] (Extended Data Fig. 5f–h). We also observed that the mRNAs that bind to TDP-43 changed significantly during skeletal muscle differentiation (Extended Data Fig. 6a).

Most of the TDP-43 binding sites in myoblasts and myotubes were found to be in exons of protein-coding transcripts, suggesting that TDP-43 could be associating with mature mRNAs (Fig. 3a and Extended Data Fig. 6b, c). By contrast, TDP-43-binding sites in neurons predominantly mapped to introns[18,19]. The difference may reflect cell state, whereby TDP-43 binds more processed cytoplasmic RNAs in newly forming tissue and more nuclear intronic RNA in post-mitotic mature cells. Connectome and Gene Ontology analysis of TDP-43 exonic target transcripts in myotubes, which are likely to constitute interactions with cytoplasmic mRNAs, revealed that TDP-43 binds to a network of transcripts associated with the sarcomere (Fig. 3b and Extended Data Fig. 6a). TDP-43 target RNAs that were identified by eCLIP in myotubes often had multiple TDP-43 exonic binding sites in close proximity[19]. For example, numerous TDP-43 exon-binding sites are distributed across the mRNA transcript of *Ttn* (which encodes titin), and we observed multiple UG-rich

Fig. 2 | Myo-granules containing TDP-43 are amyloid-like oligomers. **a**, X-ray diffraction of myo-granules immunoprecipitated from C2C12 myotubes. Two rings at approximately 4.8 Å (orange) and approximately 10 Å (blue) are drawn on the bottom half to highlight the locations of these reflections. One sample per condition was used. Two diffraction images at different rotations were taken per sample and each image showed similar results. **b**, A11 immunoreactivity in tibialis anterior muscle regeneration and uninjured muscle. $n = 4$ mice per condition. Regenerating myofibres showed eMHC expression. Scale bars, 25 μm. **c**, Quantification of A11 and TDP-43 co-localization and A11 and eMHC co-localization in skeletal muscle at 5 DPI. Unpaired, two-tailed Student's t-test, ****$P = 6.3 \times 10^{-17}$. $n = 3$ mice, $n = 5$ myofibres per mouse. Data are mean ± s.d. **d**, Representative deconvolution images of A11 and TDP-43 co-localization in mouse tibialis anterior myofibres at 5 DPI for data quantified in **c**. Scale bars, 3 μm and 1 μm (inset). $n = 3$ mice, each showing similar results.

stretches within single exons of *Ttn* with several TDP-43-binding sites (Extended Data Fig. 6d). These observations suggest that TDP-43 has a different function during myogenesis, during which TDP-43 binds to structural mRNAs that are required for skeletal muscle formation, while retaining canonical nuclear functions such as splicing and nuclear cytoplasmic shuttling.

To confirm that the sarcomeric mRNAs that were identified by eCLIP bind to cytoplasmic TDP-43 during muscle formation, we used single-molecule fluorescence in situ hybridization. We found that the TDP-43 protein co-localizes with mRNAs of *Myh3* (which encodes eMHC) and *Tnnc1* in the cytoplasm of myotubes (Fig. 3c). In addition, single-molecule fluorescence in situ hybridization of *Ttn* mRNA reveals co-localization of both TDP-43 expression and A11 immunoreactivity with *Ttn* mRNA in myotubes (Fig. 3d). These observations demonstrate that TDP-43 binds to sarcomeric mRNAs in the cytosol, and can form A11-positive myo-granules in association with those mRNAs—perhaps because of the high local concentration of TDP-43 proteins on a single mRNA molecule[19,20].

The association of TDP-43 myo-granules with sarcomeric mRNAs during muscle formation is analogous to the role of TDP-43 in forming cytoplasmic neuronal messenger ribonucleoprotein granules for local translation of mRNAs in neurons[21]. Consistent with this similarity, mass spectrometry of purified myo-granules identified 356 proteins that were enriched in proteins involved in RNA localization and translation, which overlaps with the TDP-43 interactome[22] and the neuronal RNA granule proteome[23] (Extended Data Fig. 7a–d and Supplementary Tables 1, 2). Myo-granules included valosin-containing protein (VCP), a protein that has been linked to neuromuscular degeneration[24]; we validated this by analysing the co-localization of VCP with A11 and TDP-43 in the cytoplasm of regenerating muscle (Extended Data Fig. 7e). However, HNRNPA2B1, an RNA-binding protein associated with neuromuscular degeneration[25], was not identified in myo-granules and remained in the nucleus during muscle regeneration (Extended Data Fig. 7f). Therefore, myo-granules associate with a specific set of proteins that may help to localize and regulate sarcomeric mRNAs during skeletal-muscle formation.
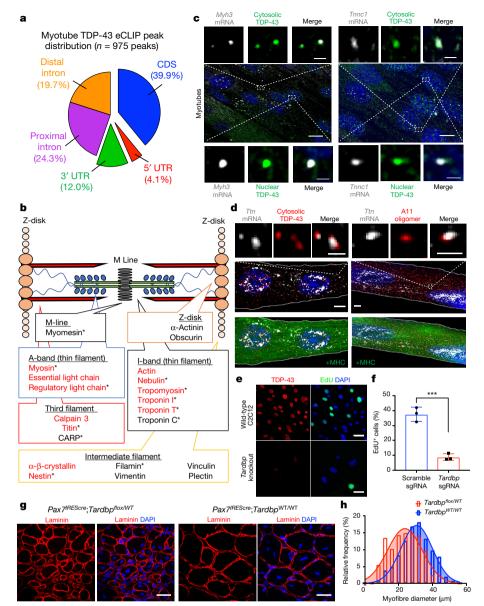
TDP–43 is essential for muscle formation

If TDP-43-containing myo-granules are sarcomeric messenger ribonucleoproteins, then genetic depletion of *Tardbp* may disrupt skeletal-muscle myofibre formation. CRISPR–Cas9-mediated deletion of *Tardbp* in C2C12 cells arrested growth of C2C12 myoblasts, which led to cell death and prevented myoblast differentiation (Fig. 3e, f and Extended Data Fig. 8a). Because TDP-43 appears to be essential for myoblast proliferation and survival, we investigated whether removing one copy of the *Tardbp* gene in muscle stem cells using *Pax7*[IREScre] recombination impaired muscle regeneration[26,27] (Extended Data Fig. 8b, c). In uninjured mice, the size of myofibres and number of muscle stem cells were unaffected when one copy of *Tardbp* was deleted from muscle stem cells (Extended Data Fig. 8d–f). However, after injury, mice with one *Tardbp* allele in muscle stem cells had significantly smaller myofibres than wild-type mice (Fig. 3g, h and Extended Data Fig. 8g–i). Because there was no detectable change in the number of muscle stem cells when one *Tardbp* allele was deleted, we hypothesize that the regeneration defect is in part because of loss of TDP-43 function during myofibre formation. Therefore, TDP-43 is essential for skeletal-muscle-cell differentiation in culture and required for skeletal-muscle regeneration.

Myo–granules in humans and disease

To determine whether cytoplasmic TDP-43 and myo-granules are conserved in human muscle regeneration, we examined human muscle biopsies from patients with different clinical and pathological features of necrotizing myopathy. For each patient, we observed increased cytoplasmic TDP-43 and A11 amyloid oligomer staining in the regenerating muscle, indicating that myo-granules form in regenerating human myofibres and are not present in non-regenerating myofibres (Fig. 4 and Extended Data Fig. 9a). It is possible that myo-granules formed during normal regeneration may seed the aggregates seen in human muscle diseases.

Because myo-granules containing TDP-43 form during human skeletal-muscle regeneration and TDP-43 aggregates are found in skeletal-muscle diseases, the increased regeneration occurring in

Fig. 3 | TDP-43 binds to select sarcomeric mRNA transcripts during muscle formation. a, Distribution of TDP-43 RNA binding identified by eCLIP in C2C12 myotubes. CDS, coding sequence; UTR, untranslated region. **b**, TDP-43 eCLIP identified exonic peaks in select sarcomeric mRNA transcripts in myotubes. All listed genes were found in at least one eCLIP replicate; *gene identified in two replicates; red, gene associated with muscle disease. Sarcomere schematic was adapted from a previous study[38]. **c**, Single-molecule fluorescence in situ hybridization showed that *Myh3* and *Tnnc1* mRNA co-localized with cytoplasmic and nuclear TDP-43 in C2C12 myotubes. $n = 3$ biologically independent experiments. **d**, Single-molecule fluorescence in situ hybridization showed that *Ttn* mRNA co-localized with both A11 and TDP-43 in the cytoplasm of MHC⁺ C2C12 myotubes. $n = 3$ biologically independent experiments. **c, d**, Scale bars, 10 μm and 0.5 μm (insets). **e**, Representative images of C2C12 cells edited using CRISPR–Cas9 and *Tardbp* scramble single-guide (sg)RNA

(top) and *Tardbp* knockout sgRNA (bottom), showing TDP-43 expression and EdU incorporation. Scale bar, 50 μm. Cells were counterstained with DAPI. $n = 3$ biologically independent experiments, each showing similar results. **f**, Quantification of EdU incorporation in *Tardbp* knockout (*Tardbp* sgRNA) and scramble-sgRNA-treated C2C12 cells after seven days in culture. $n = 3$ independent experiments. Unpaired, two-tailed Student's t-test ***$P = 0.0007$. Data are mean ± s.d. **g**, Representative images of regenerating tibialis anterior muscle at 10 DPI showing a reduction in the myofibre feret diameter in TDP-43-haploinsufficient *Pax7*[IREScre]*Tardbp*[flox/WT] mice. Laminin identifies myofibres and nuclei are counterstained with DAPI. Scale bars, 50 μm. $n = 3$ mice per condition. **h**, Frequency distribution of myofibre feret diameters in *Pax7*[IREScre]*Tardbp*[flox/WT] mice at 10 DPI compared to *Pax7*[IREScre]*Tardbp*[WT/WT] controls. More than 450 myofibres were quantified from $n = 3$ mice per genotype.

diseases may promote TDP-43 aggregation. Indeed, cytoplasmic TDP-43 aggregates in skeletal-muscle diseases are often seen in myofibres with centrally located nuclei, which is a hallmark of regeneration[1,28]. Therefore, we tested whether cytoplasmic myo-granules accumulate in newly regenerated myofibres of *Vcp* mutant mice, a model of multisystem proteinopathy and inclusion body myopathy characterized by TDP-43 aggregation[29]. When uninjured *Vcp* mutant and wild-type mice were treated with 5-ethynyl-2′-deoxyuridine (EdU), which identifies actively regenerating myofibres that contained newly fused nuclei

arising from muscle stem cells, *Vcp* mutant mice possessed more EdU⁺ centrally located myonuclei compared to *Vcp* wild-type mice (Extended Data Fig. 9b, c). Moreover, in the myofibres with EdU⁺ centrally located nuclei, we detected increased cytoplasmic TDP-43 and A11 amyloid oligomer staining, correlating cytoplasmic TDP-43 aggregation with increased muscle regeneration in *Vcp* mutant mice (Fig. 5a, b and Extended Data Fig. 9d, e).

Consistent with the hypothesis that myo-granules may seed the aggregates seen in disease, myo-granules isolated from C2C12
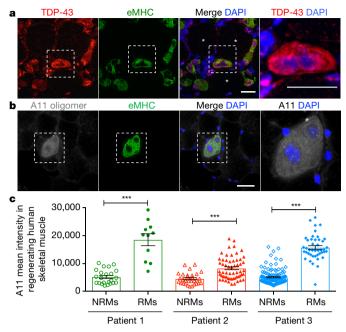
Fig. 4 | Myo-granules form during human muscle regeneration.
a, Representative images of cytoplasmic TDP-43 in regenerating human skeletal muscle from a patient with necrotizing myopathy. Asterisks, uninjured myofibres that lack eMHC and TDP-43 cytosolic signals. $n = 3$ individual patient skeletal muscle biopsies, each showing similar results. Scale bars, 50 μm. **b**, Representative image of A11 immunoreactivity in regenerating human skeletal muscle from a patient with necrotizing myopathy. $n = 3$ individual patient skeletal muscle biopsies, each showing similar results. Scale bar, 100 μm. **c**, Quantification of A11 immunoreactivity in eMHC$^+$ regenerating myofibres (RMs) compared to eMHC$^-$ non-regenerating myofibres (NRMs) from three patients with necrotizing myopathy. Unpaired, two-tailed Student's t-tests were used for each individual comparison: patient 1, NRMs ($n = 23$) versus RMs ($n = 11$), ***$P = 2.54 \times 10^{-9}$; patient 2, NRMs ($n = 31$) versus RMs ($n = 59$), ***$P = 7.89 \times 10^{-6}$; patient 3, NRMs ($n = 146$) versus RMs ($n = 44$) ***$P = 6.17 \times 10^{-49}$. Data are mean ± s.e.m.

myotubes were capable of transitioning to a thioflavin-T$^+$ aggregate (amyloid-like fibres) over time (Fig. 5c, d). Moreover, addition of recombinant TDP-43 to isolated myo-granules increased the amount of thioflavin-T$^+$ aggregates that were formed without affecting their initial rate of assembly (Fig. 5c, d and Extended Data Fig. 9f, g). TEM of thioflavin-T$^+$ TDP-43 aggregates formed from myo-granules reveals fibrous structures that are morphologically similar to previously reported TDP-43 amyloid fibres[30] (Fig. 5e). This suggests that the failure to dissipate myo-granules during normal muscle formation may seed the formation of cytoplasmic TDP-43 aggregates in diseased muscle. Whether the oligomerization of TDP-43 in myo-granules involves its N-terminal oligomerization domain[20], the C-terminal prion-like domain that is prone to aggregation and fibre formation[31,32], or both, remains to be established.

Discussion

We uncover two important properties of TDP-43 in the formation of skeletal muscle. First, TDP-43 is an essential protein that associates with select sarcomeric mRNAs and localizes to sites of newly forming sarcomeres during skeletal muscle formation. Second, TDP-43 is a component of a higher-order, amyloid-like myo-granule assembled during normal skeletal-muscle formation. Purified myo-granules from cultured myotubes are capable of seeding amyloid-like fibrils in vitro, which suggests a link between the normal biological functions of TDP-43 and pathological TDP-43 aggregates.

We propose a model in which myo-granules that contain TDP-43 are increased in damaged tissues with elevated regeneration, thereby enhancing the possibility of amyloid fibre formation and/or
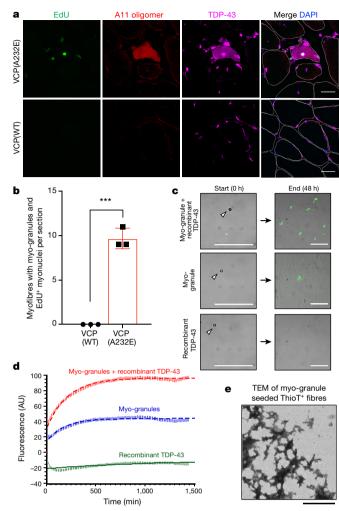
Fig. 5 | Myo-granules are increased in multisystem proteinopathy and are capable of seeding amyloid-like fibres. a, Tibialis anterior muscles from uninjured VCP(A232E) mice (top) and uninjured VCP wild-type (WT) mice (bottom) analysed for EdU incorporation into centrally located nuclei and immunostained for A11 and TDP-43. Cells were counterstained with DAPI and myofibres are outlined in white. Scale bars, 25 μm. **b**, Quantification of myofibres with EdU$^+$ centrally located myonuclei, A11 immunoreactivity and cytoplasmic TDP-43 expression in VCP(A232E) and VCP(WT) mice. Unpaired, two-tailed Student's t-test ***$P = 1.3 \times 10^{-4}$. $n = 3$ mice, one tibialis anterior cross-section was quantified per mouse. Data are mean ± s.d. and individual mice are shown. **c**, Representative images of purified myo-granules from C2C12 myotubes incubated with or without recombinant TDP-43 and Thioflavin-T (ThioT) reveals the formation of higher-order thioflavin-T$^+$ amyloid-like fibres. Arrowhead points to a bead used to determine correct focal plane at time = 0. Scale bars, 25 μm. $n = 3$ biologically independent experiments. **d**, Plot of kinetics of fibre aggregation determined by thioflavin-T incorporation measured at 10-min intervals. Rates were derived by fitting time points to a single exponential rate (equation (1); see Methods). Myo-granule + recombinant TDP-43, $R^2 = 0.96$, $k_{observed} = 47 \pm 1.6 \times 10^{-4}$ min^{-1} (mean ± s.d.) myo-granule, $R^2 = 0.92$, $k_{observed} = 56 \pm 2.9 \times 10^{-4}$ min^{-1}; recombinant TDP-43, $R^2 = 0.47$, $k_{observed} = 8.5 \pm 4.9 \times \times 10^{-4}$ min^{-1}. $n = 3$ biologically independent experiments, background-corrected arbitrary units (AU). **e**, Representative TEM images of thioflavin-T$^+$ fibres formed from isolated myo-granules. $n = 3$ biologically independent experiments. Scale bar, 1 μm.

aggregation of TDP-43 in disease (Extended Data Fig. 10). Because the triggering event in this model is elevated muscle regeneration, it explains why TDP-43 aggregates occur in genetically diverse diseases, including inclusion body myopathy[28], which can be caused by mutations in the ubiquitin segregase VCP[29]; oculopharyngeal muscular dystrophy, caused by Ala expansions in PABPN1[1]; and distal

myopathy with rimmed vacuoles, caused by mutations in the UDP-*N*-acetylglucosamine 2-epimerase gene (*GNE*)[33]. Moreover, the seeding of TDP-43 aggregates by TDP-43 oligomers may also occur in neurons as reversible cytoplasmic TDP-43 accumulation occurs in models of acute neuronal injury in vivo (for example, axotomy or traumatic brain injury)[34,35]. TDP-43 aggregates are also frequently observed on autopsy in neurologically normal elderly individuals[36]. The age-dependent accumulation of TDP-43 aggregates may be caused by a failure to clear TDP-43, or other amyloid-like assemblies that have formed during tissue repair. Over a lifetime, failures in proteostatic control mechanisms—including autophagy or endocytosis[37]—could increase the likelihood that functional, amyloid-like assemblies transition into pathological aggregates.

Online content

1. Küsters, B. et al. TDP-43 accumulation is common in myopathies with rimmed vacuoles. *Acta Neuropathol.* **117**, 209–211 (2009).
2. Weihl, C. C. et al. TDP-43 accumulation in inclusion body myopathy muscle suggests a common pathogenic mechanism with frontotemporal dementia. *J. Neurol. Neurosurg. Psychiatry* **79**, 1186–1189 (2008).
3. Neumann, M. et al. Ubiquitinated TDP-43 in frontotemporal lobar degeneration and amyotrophic lateral sclerosis. *Science* **314**, 130–133 (2006).
4. Renton, A. E., Chiò, A. & Traynor, B. J. State of play in amyotrophic lateral sclerosis genetics. *Nat. Neurosci.* **17**, 17–23 (2014).
5. Kraemer, B. C. et al. Loss of murine TDP-43 disrupts motor function and plays an essential role in embryogenesis. *Acta Neuropathol.* **119**, 409–419 (2010).
6. Schmid, B. et al. Loss of ALS-associated TDP-43 in zebrafish causes muscle degeneration, vascular dysfunction, and reduced motor neuron axon outgrowth. *Proc. Natl Acad. Sci. USA* **110**, 4986–4991 (2013).
7. Diaper, D. C. et al. *Drosophila* TDP-43 dysfunction in glia and muscle cells cause cytological and behavioural phenotypes that characterize ALS and FTLD. *Hum. Mol. Genet.* **22**, 3883–3893 (2013).
8. Llamusi, B. et al. Muscleblind, BSF and TBPH are mislocalized in the muscle sarcomere of a *Drosophila* myotonic dystrophy model. *Dis. Model. Mech.* **6**, 184–196 (2013).
9. Rodriguez-Ortiz, C. J. et al. Neuronal-specific overexpression of a mutant valosin-containing protein associated with IBMPFD promotes aberrant ubiquitin and TDP-43 accumulation and cognitive dysfunction in transgenic mice. *Am. J. Pathol.* **183**, 504–515 (2013).
10. Caldwell, C. J., Mattey, D. L. & Weller, R. O. Role of the basement membrane in the regeneration of skeletal muscle. *Neuropathol. Appl. Neurobiol.* **16**, 225–238 (1990).
11. Hardy, D. et al. Comparative study of injury models for studying muscle regeneration in mice. *PLoS ONE* **11**, e0147198 (2016).
12. Webster, C., Silberstein, L., Hays, A. P. & Blau, H. M. Fast muscle fibers are preferentially affected in Duchenne muscular dystrophy. *Cell* **52**, 503–513 (1988).
13. Johnson, B. S. et al. TDP-43 is intrinsically aggregation-prone, and amyotrophic lateral sclerosis-linked mutations accelerate aggregation and increase toxicity. *J. Biol. Chem.* **284**, 20329–20339 (2009).
14. Sangwan, S. et al. Atomic structure of a toxic, oligomeric segment of SOD1 linked to amyotrophic lateral sclerosis (ALS). *Proc. Natl Acad. Sci. USA* **114**, 8770–8775 (2017).
15. Kayed, R. et al. Common structure of soluble amyloid oligomers implies common mechanism of pathogenesis. *Science* **300**, 486–489 (2003).
16. Van Nostrand, E. L. et al. Robust transcriptome-wide discovery of RNA-binding protein binding sites with enhanced CLIP (eCLIP). *Nat. Methods* **13**, 508–514 (2016).
17. Ayala, Y. M. et al. TDP-43 regulates its mRNA levels through a negative feedback loop. *EMBO J.* **30**, 277–288 (2011).
18. Polymenidou, M. et al. Long pre-mRNA depletion and RNA missplicing contribute to neuronal vulnerability from loss of TDP-43. *Nat. Neurosci.* **14**, 459–468 (2011).
19. Tollervey, J. R. et al. Characterizing the RNA targets and position-dependent splicing regulation by TDP-43. *Nat. Neurosci.* **14**, 452–458 (2011).
20. Afroz, T. et al. Functional and dynamic polymerization of the ALS-linked protein TDP-43 antagonizes its pathologic aggregation. *Nat. Commun.* **8**, 45 (2017).
21. Alami, N. H. et al. Axonal transport of TDP-43 mRNA granules is impaired by ALS-causing mutations. *Neuron* **81**, 536–543 (2014).
22. Freibaum, B. D., Chitta, R. K., High, A. A. & Taylor, J. P. Global analysis of TDP-43 interacting proteins reveals strong association with RNA splicing and translation machinery. *J. Proteome Res.* **9**, 1104–1120 (2010).
23. El Fatimy, R. et al. Tracking the fragile X mental retardation protein in a highly ordered neuronal ribonucleoparticles population: a link between stalled polyribosomes and RNA granules. *PLoS Genet.* **12**, e1006192 (2016).
24. Taylor, J. P. Multisystem proteinopathy: intersecting genetics in muscle, bone, and brain degeneration. *Neurology* **85**, 658–660 (2015).
25. Kim, H. J. et al. Mutations in prion-like domains in *hnRNPA2B1* and *hnRNPA1* cause multisystem proteinopathy and ALS. *Nature* **495**, 467–473 (2013).
26. Chiang, P.-M. et al. Deletion of *TDP-43* down-regulates *Tbc1d1*, a gene linked to obesity, and alters body fat metabolism. *Proc. Natl Acad. Sci. USA* **107**, 16320–16324 (2010).
27. Murphy, M. M., Lawson, J. A., Mathew, S. J., Hutcheson, D. A. & Kardon, G. Satellite cells, connective tissue fibroblasts and their interactions are crucial for muscle regeneration. *Development* **138**, 3625–3637 (2011).
28. Salajegheh, M. et al. Sarcoplasmic redistribution of nuclear TDP-43 in inclusion body myositis. *Muscle Nerve* **40**, 19–31 (2009).
29. Custer, S. K., Neumann, M., Lu, H., Wright, A. C. & Taylor, J. P. Transgenic mice expressing mutant forms VCP/p97 recapitulate the full spectrum of IBMPFD including degeneration in muscle, brain and bone. *Hum. Mol. Genet.* **19**, 1741–1755 (2010).
30. Mompeán, M. et al. Structural evidence of amyloid fibril formation in the putative aggregation domain of TDP-43. *J. Phys. Chem. Lett.* **6**, 2608–2615 (2015).
31. Chen, A. K.-H. et al. Induction of amyloid fibrils by the C-terminal fragments of TDP-43 in amyotrophic lateral sclerosis. *J. Am. Chem. Soc.* **132**, 1186–1187 (2010).
32. Igaz, L. M. et al. Expression of TDP-43 C-terminal fragments in vitro recapitulates pathological features of TDP-43 proteinopathies. *J. Biol. Chem.* **284**, 8516–8524 (2009).
33. Nishino, I. et al. Distal myopathy with rimmed vacuoles is allelic to hereditary inclusion body myopathy. *Neurology* **59**, 1689–1693 (2002).
34. Wiesner, D. et al. Reversible induction of TDP-43 granules in cortical neurons after traumatic injury. *Exp. Neurol.* **299**, 15–25 (2018).
35. Moisse, K. et al. Divergent patterns of cytosolic TDP-43 and neuronal progranulin expression following axotomy: implications for TDP-43 in the physiological response to neuronal injury. *Brain Res.* **1249**, 202–211 (2009).
36. Wilson, R. S. et al. TDP-43 pathology, cognitive decline, and dementia in old age. *JAMA Neurol.* **70**, 1418–1424 (2013).
37. Liu, G. et al. Endocytosis regulates TDP-43 toxicity and turnover. *Nat. Commun.* **8**, 2092 (2017).
38. Laing, N. G. & Nowak, K. J. When contractile proteins go bad: the sarcomere and skeletal muscle disease. *BioEssays* **27**, 809–822 (2005).

Author contributions T.O.V., J.R.W., B.B.O. and R.P. conceived and designed the research, wrote the manuscript and all authors edited drafts. T.O.V., J.R.W., E.L., N.D.B. and O.N.W. performed and analysed mouse regeneration and myotube formation experiments. J.R.W. and E.L. isolated myo-granules. T.E.E., J.R.W. and T.O.V. analysed HaloTag–TDP-43. M.P.H., J.R.W. and T.O.V. performed X-ray diffraction and TEM. E.D.N. and J.R.W. performed eCLIP analysis. T.O.V. and K.A.B. analysed human biopsies. T.O.V. performed VCP experiments. J.R.W. and B.R. performed thioflavin-T assays. E.G., J.S., T.E.L., D.S.E., J.P.T. and A.M.J. provided scientific insights and materials.

METHODS

Mice. Mice were bred and housed according to National Institutes of Health (NIH) guidelines for the ethical treatment of animals in a pathogen-free facility at the University of Colorado at Boulder (wild-type, $Pax7^{IREScre}$, $Tardbp^{flox/flox}$ and VCP(A232E) lines). The University of Colorado Institutional Animal Care and Use Committee (IACUC) approved all animal protocols and procedures and studies complied with all ethical regulations. Wild-type mice were C57BL/6 (Jackson Laboratories) and VCP(A232E), VCP(WT)[29], and $Tardbp^{flox/flox}$ mice[26] were previously described. Crossing mice into $Pax7^{IREScre}$ mice[27] generated conditional $Tardbp^{flox/WT}$ mice. Cells and tibialis anterior muscles were isolated from 3–6-month-old male and female wild-type and $Pax7^{IREScre}Tardbp^{flox/WT}$ mice. Tibialis anterior or gastrocnemius muscles were isolated from nine-month-old male VCP(A232E) mice. Control mice were randomly assigned and were age- and sex-matched to the mice and crosses described above. Sample sizes were set at $n = 3$ unless otherwise noted. No statistical methods were used to predetermine sample size.

Mouse injuries and tamoxifen injections. Mice at 3–6 months old were anaesthetized with isofluorane and the left tibialis anterior muscle was injected with 50 μl of 1.2% BaCl$_2$ and then the injured and contralateral tibialis anterior muscles were collected at the indicated time points. Tamoxifen (Sigma-Aldrich), resuspended in sterile corn oil (Sigma-Aldrich), was administered by intraperitoneal injection to 3–6-month-old mice at a volume of 0.075 mg of tamoxifen per gram of mouse weight. Muscle injuries were made blinded to genotype.

Human muscle biopsy tissue. Under an IRB-approved protocol at Johns Hopkins University and complying with all ethical regulations, a clinical muscle biopsy database was searched for patients who had been clinically diagnosed with rhabdomyolysis and/or pathologically diagnosed with necrotizing myopathy with evidence of myofibre regeneration. Muscle biopsy specimens used in this study were left over from diagnostic biopsies and the IRB approved that patient consent was not necessary. Patient muscle tissue leftover from the diagnostic biopsy was stored frozen at −80 °C for less than two years, and samples were cryo-sectioned for immunohistochemical analysis.

Immunofluorescence staining of tissue sections. Tibialis anterior or gastrocnemius muscles were dissected, fixed on ice for 2 h with 4% paraformaldehyde, and then transferred to phosphate-buffered saline (PBS) with 30% sucrose at 4 °C overnight. Muscle was mounted in OCT (Tissue-Tek) and cryo-sectioning was performed on a Leica cryostat to generate 10-μm thick sections. Tissues and sections were stored at −80 °C until staining. Tissue sections were post-fixed in 4% paraformaldehyde for 10 min at room temperature and washed three times for 5 min in PBS. Immunostaining with anti-PAX7, anti-laminin, anti-eMHC, anti-TDP-43 and A11 antibodies required heat-induced epitope retrieval, for which post-fixed slides were placed in citrate buffer, pH 6.0, and subjected to 6 min of high pressure-cooking in a Cuisinart model CPC-600 pressure cooker. For immunostaining, tissue sections were permeabilized with 0.25% Triton X-100 (Sigma-Aldrich) in PBS containing 2% bovine serum albumin (BSA) (Sigma-Aldrich) for 60 min at room temperature. Incubation with primary antibody occurred at 4 °C overnight followed by incubation with the secondary antibody at room temperature for 1 h. Primary antibodies included mouse anti-PAX7 (Developmental Studies Hybridoma Bank) at 1:750, rabbit anti-laminin (Sigma-Aldrich) at 1:200, rabbit anti-TDP-43 (ProteinTech) at 1:200, mouse anti-TDP-43 (Abcam) at 1:200, rabbit A11 (Sigma-Aldrich) at 1:200, mouse anti-VCP (ThermoFisher Scientific) at 1:400 and mouse anti-eMHC (Developmental Studies Hybridoma Bank) at 1:5. Alexa secondary antibodies (Molecular Probes) were used at a dilution of 1:1,000. For analysis that included EdU detection, EdU staining was completed before antibody staining using the Click-iT EdU Alexa Fluor 488 detection kit (Molecular Probes) following the manufacturer's protocols. Sections were incubated with 1 μg ml^{-1} DAPI for 10 min at room temperature then mounted in Mowiol supplemented with DABCO (Sigma-Aldrich) or ProLong Gold (Thermo) as an anti-fade agent.

Isolation of primary muscle stem cells. Gastrocnemius, extensor digitorum longus, tibialis anterior and all other lower hindlimb muscles were dissected from wild-type mice. The muscle groups from both hindlimbs were separated and digested in 3.6 ml of F12-C (Gibco) with penicillin and streptomycin (Gibco) and 400 μl 10× collagenase (Worthington) for 90 min at 37 °C on a slow rotisserie. In a biosafety cabinet, muscles allowed to settle for 5 min, undisturbed. Then, as much of the liquid as possible was removed without disturbing the muscle groups. F12-C with penicillin and streptomycin and 15% horse serum was added and the muscles were rocked for 1 min. Then, 3 ml of growth medium was added to each tube (F12-C with penicillin and streptomycin, 15% horse serum (Gibco), 20% fetal bovine serum (Sigma-Aldrich), 1% chick embryo extract (Antibody Production Services). The digest was poured onto a 10-cm tissue-culture plate (Corning) with Matrigel in 10 ml of growth medium. Growth medium was added as necessary to keep the muscle chunks submerged. Muscles chunks were incubated in growth medium with FGF-2 (50 nM working concentration) for 72 h at 37 °C in 6% O$_2$ and 5% CO$_2$. After 72 h, muscle stem cells had migrated out onto the Matrigel and

the muscle chunks and medium were removed. The plate containing attached muscle stem cells was rinsed with sterile PBS and 10 ml warm growth medium was added supplemented with 50 nM FGF-2. Colonies of myoblasts formed by four days of culture and were expanded by passaging with 0.25% trypsin-EDTA (Sigma-Aldrich).

Cell culture. *Primary muscle stem cells.* After initial isolation, primary myoblasts were maintained on Matrigel-coated tissue-culture plastic plates or gelatin-coated coverslips at 37 °C at 6% O$_2$ and 5% CO$_2$ in growth medium as described above. Medium was changed only during cell passaging. To promote myoblast fusion, cells at 75% confluency were washed three times with PBS and the medium was switched to DMEM (Gibco) with 5% horse serum (Gibco), 1% penicillin and streptomycin and 1% insulin–transferrin–selenium (Gibco). To induce stress-granule formation, primary myotubes were stressed with 0.5 mM sodium arsenite for 1 h at 37 °C.

C2C12 cells. Immortalized mouse myoblasts (American Type Culture Collection) were maintained on uncoated standard tissue-culture plastic or gelatin-coated coverslips at 37 °C with 5% CO$_2$ in DMEM with 20% fetal bovine serum and 1% penicillin and streptomycin. To promote myoblast fusion when the C2C12 cells reached confluence, they were switched to 5% horse serum, 1% penicillin and streptavidin and 1% insulin–transferrin–selenium in DMEM. To induce stress-granule formation, C2C12 myotubes were stressed with 0.5 mM sodium arsenite for 1 h at 37 °C.

U2-OS cells. Human osteosarcoma cells were maintained in DMEM, high glucose, GlutaMAX with 10% fetal bovine serum, 1% penicillin–streptomycin and 1 mM sodium pyruvate at 37 °C and 5% CO$_2$.

Yeast. For the experiments presented in Fig. 1, BY4741 yeast was transformed with a single plasmid expressing Pub1Q/N-GFP (pRP1689) (laboratory of R.P.) and grown at 30 °C in minimal medium with 2% glucose as a carbon source and with leucine dropout to maintain the plasmid. For experiments presented in Supplementary Fig. 3, SUP35 [PSI+] (5V-H19A) and SUP35 [psi−] (yAV831) stains were grown in minimal medium with a complete set of amino acids and 2% dextrose at 30 °C.

Immunofluorescence staining of cells and proximity ligation assay. Primary and immortalized cells were washed with PBS in a laminar flow hood and fixed with 4% paraformaldehyde for 10 min at room temperature in a chemical hood. Cells were permeabilized with 0.25% Triton X-100 in PBS containing 2% BSA (Sigma-Aldrich) for 1 h at room temperature. Incubation with primary antibody occurred at 4 °C overnight followed by incubation with the secondary antibody at room temperature for 1 h. Primary antibodies included mouse anti-PAX7 (Developmental Studies Hybridoma Bank) at 1:750, rabbit anti-TDP-43 (ProteinTech) at 1:200, mouse anti-TDP-43 (Abcam) at 1:200, rabbit A11 (Sigma-Aldrich) at 1:200 and mouse anti-MHC (MF-20, Developmental Studies Hybridoma Bank) at 1:1. Alexa secondary antibodies (Molecular Probes) were used at a dilution of 1:1,000. All antibodies were diluted in 0.125% Triton X-100 in PBS containing 2% BSA. For analysis that included EdU detection, EdU staining was completed before antibody staining using the Click-iT EdU Alexa Fluor 488 detection kit (Molecular Probes) following the manufacturer's protocol. Cells were incubated with 6.6 mM phalloidin (Thermo Scientific) for 20 min and/or 1 μg ml^{-1} DAPI for 10 min at room temperature then mounted in Mowiol supplemented with DABCO (Sigma-Aldrich) as an anti-fade agent.

For the proximity ligation assay, samples were incubated with indicated antibodies at the concentrations listed above. Secondary antibody incubation and Duolink proximity ligation assays were performed according to the manufacturer's protocol (Sigma-Aldrich).

Subcellular fractionation. Nuclear/cytosolic fractionation was performed to determine localization of soluble TDP-43 in C2C12 myoblasts and differentiating myotubes. In brief, myoblasts or differentiating myotubes (day 4) were trypsinized, washed with PBS and pelleted by centrifugation at 1,000g for 5 min. Cells were subsequently washed in PBS and divided into a whole-cell lysate fraction (1/3 total) or a cytosolic/nuclear fraction (2/3 total). Both cellular fractions were pelleted by centrifugation at 1,000g for 5 min. The whole-cell lysate fraction was resuspended into RIPA buffer (50 mM Tris pH 7.5, 1% NP-40, 0.5% sodium deoxycholate, 0.05% SDS, 1 mM EDTA, 150 mM NaCl and protease inhibitors (Roche)) and placed on ice. The cytosolic/nuclear fraction was resuspended in a hypotonic lysis buffer (10 mM Tris HCL 7.5, 10 mM NaCl, 3 mM MgCl$_2$, 0.5% NP40 and protease inhibitors (Roche)) and placed on ice for 4 min. Nuclei were then pelleted by centrifugation at 500g for 5 min. The supernatant (cytosolic fraction) was removed. The pellet (nuclear fraction) was then resuspended in nuclear lysis buffer (50 mM Tris HCl 7.4, 120 mM NaCl, 1% SDS, 1 mM EDTA, 50 mM DTT and protease inhibitors (Roche)). Nuclei were lysed with five passages through an 18G needle. Cellular debris was cleared from collected fractions with centrifugation at 1,000g for 5 min. Equal volumes (20 μl) of fractions were then resolved on a 4–12% Bis-Tris SDS–PAGE gel and transferred to a nitrocellulose membrane (Bio-Rad). Western blotting was performed according to standard procedures.

Single molecule imaging of endogenous HaloTag–TDP-43. A tetracycline-inducible HaloTag (Promega) TDP-43 fusion protein was knocked into the *Rosa26* safe-harbour locus using CRISPR–Cas9[39]. Knockin cells were selected using puromyocin and proper genomic integration was confirmed by PCR and western blotting. For live-cell single-molecule imaging studies, puromyocin-resistant myoblasts or differentiating myotubes were grown on collagen-treated, 35-mm imaging dishes (MatTek). HaloTag–TDP-43 was induced for 48 h using doxycycline (1 µg ml^{-1}). HaloTag–TDP-43 molecules were labelled with 50 pM JF646 dye (gift from L. Lavis) for 15 min in culture medium[40]. After the pulse, cells were washed three times with medium and incubated with vibrant violet (1:400) in medium to visualize myonuclei for at least 1 h before image acquisition. All single-molecule live imaging was performed under HILO conditions (highly inclined and laminated optical sheet) on a Nikon N-STORM microscope equipped with TIRF illuminator, an environmental chamber, two iXon Ultra 897 EMCCD cameras (Andor), a 100× oil-immersion objective (Nikon, NA 1.49), two filter wheels, appropriate filter sets, and 405 nm (20 mW), 488 nm (50 mW), 561 nm (50 mW), and 647 nm (125 mW) laser lines. Differentiating myotubes were identified by visualizing fused myonuclei with a 405 nm laser line (1% laser power). To image HaloTag–TDP-43, cells were imaged continuously with 647 nm (40% laser power) for 15 s at an effective frame rate of 100 frames per s. Single-particle tracks were generated using MATLAB.

Biochemical characterization of TDP-43 during myogenesis. For RIPA/urea solubility assays, C2C12 myoblasts and myotubes were lysed with RIPA buffer (50 mM Tris pH 7.5, 1% NP-40, 0.5% sodium deoxycholate, 0.05% SDS, 1 mM EDTA, 150 mM NaCl). Protein concentrations were determined using BCA assay (Thermo Scientific) according to standard procedures. Lysates were centrifuged at 18,000g for 20 min at 4 °C. The supernatant represented the RIPA-soluble fraction while the pellet was solubilized in 7 M urea in TBE and represents the urea-soluble fraction. Western blotting was performed following resolution of protein lysates on SDS–PAGE.

Semi-denaturing detergent–agarose gel electrophoresis (SDD–AGE) was conducted as previously described[41]. In brief, C2C12 myoblasts and myotubes were lysed with RIPA buffer, protein concentrations were standardized using BCA assay, diluted to 1× in loading buffer (2× TAE, 20% glycerol, 8% SDS and bromophenol blue) and separated across a 1.5% agarose gel containing 0.1% SDS. Gels were transferred by capillary transfer overnight to nitrocellulose in TBS. Standard western blotting procedures were used.

For fractionation of TDP-43 oligomers across sucrose gradients (10–35%), fractions were collected and equal volumes were loaded for SDD–AGE analysis. Immunoprecipitation followed by scanning electron microscopy of the TDP-43 SDS-resistant fraction was performed as described below.

Dot blots of C2C12 protein lysates or whole-muscle lysates were conducted according to standard procedures[42]. Both C2C12 cells and whole muscle were lysed in RIPA buffer, protein concentrations were normalized using BCA and were spotted onto nitrocellulose membranes.

Isolation of myo-granules. A protocol for isolating myo-granules from myotubes was modified from existing protocols for isolating heavy ribonucleoprotein complexes[43]. In brief, myotubes or whole tibialis anterior muscles were lysed under non-denaturing conditions using CHAPS lysis buffer (10 mM Tris-HCl pH 7.5, 1 mM MgCl$_2$, 1 mM EGTA, 0.5% CHAPS, 10% glycerol, 1 mM PMSF and 1 mM DTT) or RIPA buffer and spun to remove heavy cellular debris (250g for 5 min). Successive centrifugation was used to enrich for heavy complexes (18,000g for 20 min). The pellet was resuspended into immunoprecipitation buffer (10 mM Tris HCL 7.5, 25 mM NaCl and 0.005% NP40) to create the 'myo-granule-enriched fraction'. The enriched fraction was precleared for 30 min with immunoprecipitation buffer-equilibrated Dynabeads and then incubated overnight with either antibodies against TDP-43 (Proteintech) or the A11 antibody (laboratory of C. Glabe). Myo-granules were immunopurified on equilibrated Dynabeads, washed in immunoprecipitation buffer, and eluted using Pierce Gentle Ag/Ab Buffer (Thermo Scientific) as previously described[42]. Buffer was exchanged using a 10K MW spin column (Millipore Amicon).

RNA extraction and oligo-dT northern blot analysis of myo-granules. RNA was isolated from myo-granules bound to Dynabeads by Trizol extraction followed by ethanol precipitation. RNA was run on a 1.25% formaldehyde agarose gel, transferred to nitrocellulose membrane and hybridized with a αP^{32}-labelled oligo-dT probe at room temperature overnight. Membranes were exposed on a phosphorimager screen either for 1 h (low exposure) or overnight (high exposure) and imaged on a Typhoon FLA 9500 phosphorimager.

TEM. TEM sample preparation and image acquisition was performed as previously described unless otherwise specified[44]. For experiments in which immunofluorence on TEM grids was performed, Carbon type B 300 mesh Copper TEM grids (Ted Pella) were poly-lysine-treated (Sigma-Aldrich) for 30 min, washed three times in PBS, and immunopurified myo-granules (diluted 1:50) were allowed to adhere to the grid for 1 h at room temperature. TEM grids with myo-granules were

blocked in 3% BSA for 1 h at room temperature. Primary antibody incubation was performed at a dilution of 1:100 in 3% BSA for 1 h at room temperature. Grids were then washed three times in PBS and incubated with secondary antibodies at 1:250 dilution in 3% BSA. Secondary antibody-only controls were performed at the same concentration without addition of primary antibodies. Grids were washed three times with PBS and placed onto microscopy slides. Images were acquired using a DeltaVision Elite microscope with a 100× objective. Grids were stained with uranyl acetate and immunopositive myo-granules were examined by TEM.

Myo-granule electron diffraction. Lyophilized myo-granules and SOD1 segment oligomers (prepared as previously described[14]) were mounted for diffraction by dipping a nylon loop in glycerol and sticking some of the lyophilized sample onto the glycerol[45]. Samples were carefully aligned to avoid the nylon loop entering the X-ray beam when diffraction images were taken. All samples were shot at the Advanced Photon Source (Argonne National Laboratory) beamline 24-E with a 50-µm aperture. Samples were rotated 5 degrees over a 4-s exposure at 295 K and images were analysed with ADXV.

TDP-43 eCLIP sequencing. C2C12 myoblasts were seeded at 6×10^6 cells per 15-cm plate, grown for 24 h at 37 °C, 5% CO$_2$ and either collected (undifferentiated myoblasts) or differentiated in differentiation medium for seven days. TDP-43 eCLIP was performed according to established protocols[16].

In brief, TDP-43–RNA interactions were stabilized with ultraviolet-light crosslinking (254 nm, 150 mJ cm^{-2}). Cell pellets were collected and snap-frozen in liquid nitrogen. Cells were thawed, lysed in eCLIP lysis buffer (50 mM Tris-HCl pH 7.4, 100 mM NaCl, 1% NP-40, 0.1% SDS, 0.5% sodium deoxycholate and 1× protease inhibitor) and sonicated (Bioruptor). Lysate was RNase I-treated (Ambion, 1:25) to fragment RNA. Protein–RNA complexes were immunoprecipitated using the indicated antibody. One size-matched input library was generated per biological replicate using an identical procedure without immunoprecipitation. Stringent washes were performed as described, RNA was dephosphorylated (FastAP, Fermentas), T4 PNK (NEB), and a 3′-end RNA adaptor was ligated with T4 RNA ligase (NEB). Protein–RNA complexes were resolved on an SDS–PAGE gel, transferred to nitrocellulose membranes and RNA was extracted from membrane. After RNA precipitation, RNA was reverse-transcribed using SuperScript IV (Thermo Fisher Scientific), free primers were removed, and a 3′ DNA adaptor was ligated onto cDNA products with T4 RNA ligase (NEB). Libraries were PCR-amplified and dual-indexed (Illumina TruSeq HT). Pair-end sequencing was performed on Illumina NextSeq sequencer.

Bioinformatics and statistical analysis. Read processing and cluster analysis for TDP-43 eCLIP was performed as previously described[16]. Read processing and cluster analysis for TDP-43 eCLIP was performed as previously described. In brief, 3′ barcodes and adaptor sequences were removed using standard eCLIP scripts. Reads were trimmed, filtered for repetitive elements and aligned to the mm9 reference sequence using STAR. PCR duplicate reads were removed based on the read start positions and randomer sequence. Bigwig files for genome browser display were generated based on the location of the second of the paired-end reads. Peaks were identified using the encode_branch version of CLIPPER using the parameter '-s mm9'. Peaks were normalized against size-matched input by calculating fold enrichment of reads in immunoprecipitated samples versus input, and were deemed significant if the number of reads in the immunoprecipitated sample was greater than in the input sample, with a Bonferroni-corrected Fisher exact P value less than 10^{-8}.

Microscopy and image analyses. Images were captured on a Nikon inverted spinning disk confocal microscope or a DeltaVision Elite microscope. Objectives used on the Nikon were: 10×/0.45 NA Plan Apo, 20×/0.75 NA Plan Apo and 40×/0.95 NA Plan Apo. Confocal stacks were projected as maximum intensity images for each channel and merged into a single image. Brightness and contrast were adjusted for the entire image as necessary. Both muscle stem cell numbers and average fibre diameter were counted manually using Fiji ImageJ. Objectives used on the DeltaVision Elite microscope were 100× using a PCO Edge sCMOS camera. At least three images were taken for each experiment comprising 8–10 z sections each. Images were processed using Fiji ImageJ. For super-resolution imaging, microscopy was performed using a Leica TCS SP8 White Light Laser with 63× 1.4 NA oil objective coupled to HyVolution (SVI Huygens-based deconvolution) and special Leica Hybrid Detectors. Image quantification was performed using Imaris imaging software.

Sequential immunofluorescence and single-molecule fluorescence in situ hybridization. Sequential immunofluorescence and single-molecule fluorescence in situ hybridization on fixed myotubes was performed. In brief, C2C12 myotubes were differentiated for seven days in differentiation medium, fixed in 4% paraformaldehyde (4%) for 10 min and washed in PBS. The following antibodies were used for immunofluorescence: rabbit anti-TDP-43 (Proteintech, 1:400), rabbit anti-A11 oligomer (Thermo Fisher Scientific, 1:400), goat anti-rabbit Alexa 647 (Abcam, 1:1,000), goat anti-mouse IgG1 Alexa 488 (Thermo Fisher Scientific, 1:1,000). All immunofluorescence experiments were performed sequentially except for staining

with mouse anti-myosin heavy chain, F59 (DSHB) which was diluted (1:10) in hybridization buffer. Custom Stellaris FISH probes were designed against mouse *Ttn*, *Myh3*, *Tnnc1* and probes were labelled with Quasar 570 Dye using Stellaris RNA FISH Probe Designer (Biosearch Technologies).

Mass spectroscopy. Mass spectrometry (MS) was performed as previously described[43]. In brief, samples were immunoprecipitated on Dynabeads as described above. Samples were washed with 0.1 M ammonium bicarbonate, and resuspended in 100 μl of 0.1 M ammonium bicarbonate, 0.2% sodium deoxycholate and 6 M guanidine HCL. Samples were reduced and alkylated with 5 mM TCEP, 40 mM chloroacetamide at 65 °C for 20 min in darkness. Samples were trypsinized with 0.5 μg of trypsin at 37 °C for overnight. The proteolysis reaction was quenched by acidification using formic acid. Deoxycholic acid was removed by phase-transfer using ethyl acetate. Tryptic peptides were desalted using in-house stop-and-go extraction (STAGE) tips, speed-vac to dryness and samples were stored at −80 °C.

Samples were resolved by ultra-performance liquid chromatography in the direct injection mode using a Waters nanoACQUITY system. Samples were resuspended in 12 μl of buffer A (0.1% formic acid/water), of which 5 μl (42% of total) was loaded onto a Symmetry C18 nanoACQUITY trap column (130 Å, 5 μm, 180 μm × 20 mm) with 15 μl min^{-1} of 99.5% buffer A and 0.5% buffer B (0.1% formic acid/acetonitrile) for 3 min. Samples were then eluted and resolved on a BEH130 C18 analytical column (130 Å, 1.7 μm, 75 μm × 250 mm) using a gradient with 3–8% buffer B between 0 and 3 min, 8–28% buffer B between 2 and 185 min, and 28–60% buffer B between 185 and 190 min (0.3 μl min^{-1}). MS/MS was performed using an LTQ Orbitrap Velos, scanning mass spectrometry between 400 and 1,800 m/z (1×10^6 ions, 60,000 resolution) in Fourier Transform, and selecting the 20 most intense MH_2^{2+} and MH_3^{3+} ions for MS/MS in linear trap quadropole with 180 s dynamic exclusion, 10 p.p.m. exclusion width, repeat count = 1. Maximal injection time was 500 ms for FT precursor scans with one microscan, and 250 ms for LTQ–MS/MS with one microscan and automated gain control 1×10^4. The normalized collision energy was 35%, with activation $Q = 0.25$ for 10 ms.

Raw data from mass spectrometry were processed using MaxQuant/Andromeda (version 1.5.0.12) and searched against the Uniprot mouse database (downloaded in October 2015, 46,471 entries) with common contaminant entries. The search used trypsin specificity with maximum two missed cleavages, included carbamidomethylation on Cys as a fixed modification, and N-terminal acetylation and oxidation on Met as variable modifications. Andromeda used 7 p.p.m. maximum mass deviation for the precursor ion, and 0.5 Da as MS/MS tolerance, searching eight top MS/MS peaks per 100 Da. False discovery rates were set to 0.01 for both protein and peptide identifications, with a minimum peptide length of seven amino acids, and two minimum total peptides.

***Tardbp* CRISPR–Cas9 knockout and EdU incorporation.** CRISPR–Cas9 knockout was performed in C2C12 myoblasts. sgRNAs against TDP-43 (5′-GTGTATGAGAGGAGTCCGAC-3′) were designed using CRISPR Design version 1 (http://crispr.mit.edu/) and cloned into pSpCas9(BB)-2A-Puro (PX459). T7 endonuclease assays was used to confirm correct targeting to the *Tardbp* locus. C2C12 myoblasts were transfected with JetPrime using standard protocols. Myoblasts were selected with puromyocin (1 μg ml^{-1}) for one week. C2C12 myoblasts were incubated with 10 μM EdU (Life Technologies) for 3 h. Cells were washed, fixed and stained using the methods described above.

Recombinant TDP-43 purification. Full-length human TDP-43 was subcloned into pE-SUMO (LifeSensors). His6–SUMO N-terminally tagged TDP-43 was transformed in BL21(DE3)RIL *Escherichia coli*, which were grown up from an overnight culture in LB containing ampicillin at 37 °C until an optical density at 600 nm (OD$_{600}$) of 0.3 was reached. At this time, the culture was shifted to 15 °C and grown until the OD$_{600}$ was 0.4–0.5. TDP-43 was then induced with 1 mM IPTG for 16 h at 15 °C. The *E. coli* cells were then lysed by sonication on ice in 50 mM HEPES (pH 7.5), 2% Triton X-100, 500 mM NaCl, 30 mM imidazole, 5% glycerol, 2 mM β-mercaptoethanol and protease inhibitors (cOmplete, EDTA-free, Roche). TDP-43 was purified over Ni-NTA agarose beads (Qiagen) and eluted from the beads using 50 mM HEPES (pH 7.5), 500 mM NaCl, 300 mM imidazole, 5% glycerol and 5 mM DTT. The protein was subsequently buffer-exchanged into 50 mM HEPES (pH 7.5), 500 mM NaCl, 5% glycerol and 5 mM DTT, flash-frozen in liquid nitrogen and stored as aliquots at −80 °C until use. Protein concentrations were determined by Bradford assay (Bio-Rad). The purity of TDP-43 was confirmed on a 4–20% polyacrylamide gel.

Thioflavin-T incorporation. Myo-granules were isolated from myotubes and diluted in PBS. Three separate biological replicates were performed constituting purification from three separate myotube cultures. First, 25 μM thioflavin-T (Abcam) was added to recombinant 15 μM HIS–SUMO–TDP-43, myo-granules or myo-granules plus recombinant 15 μM HIS–SUMO–TDP-43. Subsequently, surface denaturation was performed with continuous shaking at 37 °C and thioflavin-T incorporation was then monitored every 10 min at 495 nm after excitation at 438 nm on a Gen5 microplate reader (BioTek). Finally, raw fluorescence values that were obtained for experimental conditions were background subtracted and plotted as a function of time. The resulting curves were fit to following a single exponential rate equation using Kaleidagraph (Synergy Software):

$$-A e^{(-k_{obs}t)} + B \qquad (1)$$
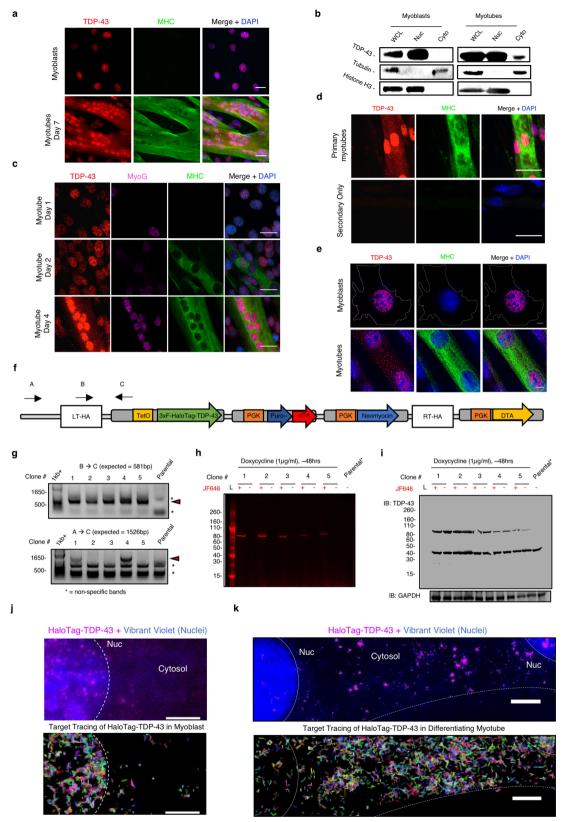
in which A is the amplitude, k_{obs} (min^{-1}) is a single exponential rate constant and B represents the maximal amount of fluorescence detected.

Reporting summary. Further information on research design is available in the Nature Research Reporting Summary linked to this paper.
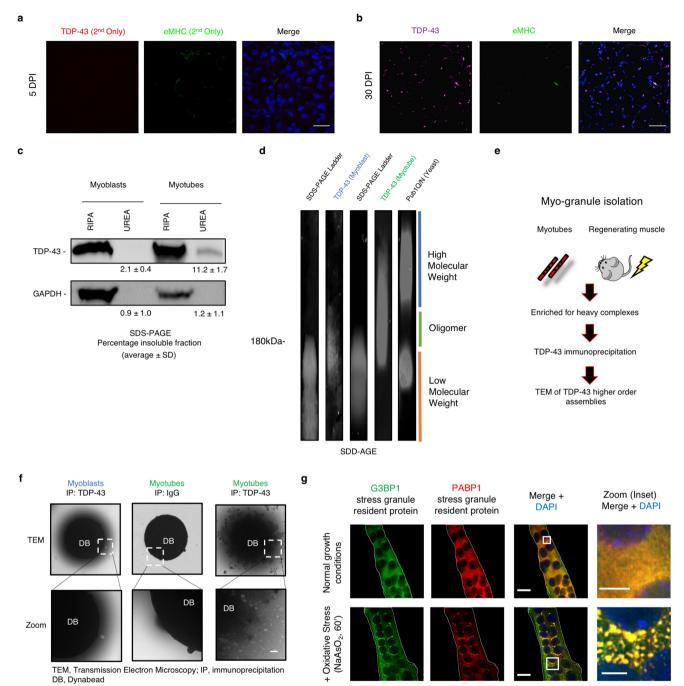
Data availability

eCLIP data are available from the Gene Expression Omnibus (GEO) under accession number GSE104796. Source Data are provided for Figs. 1d, 2c, 3f, h, 4c, 5b, c and Extended Data Figs. 1b, 2c, 3i–k, 4g, 7c, f, h, i, 8c, 9c. All other data supporting the findings of this study are available in the Supplementary Information. Data are available upon request from the corresponding authors.

39. Platt, R. J. et al. CRISPR–Cas9 knockin mice for genome editing and cancer modeling. *Cell* **159**, 440–455 (2014).
40. Grimm, J. B. et al. A general method to improve fluorophores for live-cell and single-molecule microscopy. *Nat. Methods* **12**, 244–250 (2015).
41. Halfmann, R. & Lindquist, S. Screening for amyloid aggregation by semi-denaturing detergent–agarose gel electrophoresis. *J. Vis. Exp.* **17**, 838 (2008).
42. Fang, Y.-S. et al. Full-length TDP-43 forms toxic amyloid oligomers that are present in frontotemporal lobar dementia-TDP patients. *Nat. Commun.* **5**, 4824 (2014).
43. Jain, S. et al. ATPase-modulated stress granules contain a diverse proteome and substructure. *Cell* **164**, 487–498 (2016).
44. Winey, M., Meehl, J. B., O'Toole, E. T. & Giddings, T. H. Jr. Conventional transmission electron microscopy. *Mol. Biol. Cell* **25**, 319–323 (2014).
45. Lovci, M. T. et al. Rbfox proteins regulate alternative mRNA splicing through evolutionarily conserved RNA bridges. *Nat. Struct. Mol. Biol.* **20**, 1434–1442 (2013).
46. Arnauld, S., Bertaux, N., Rigneault, H. & Marguet, D. Dynamic multiple-target tracing to probe spatiotemporal cartography of cell membranes. *Nat. Methods* **5**, 687–694 (2008).
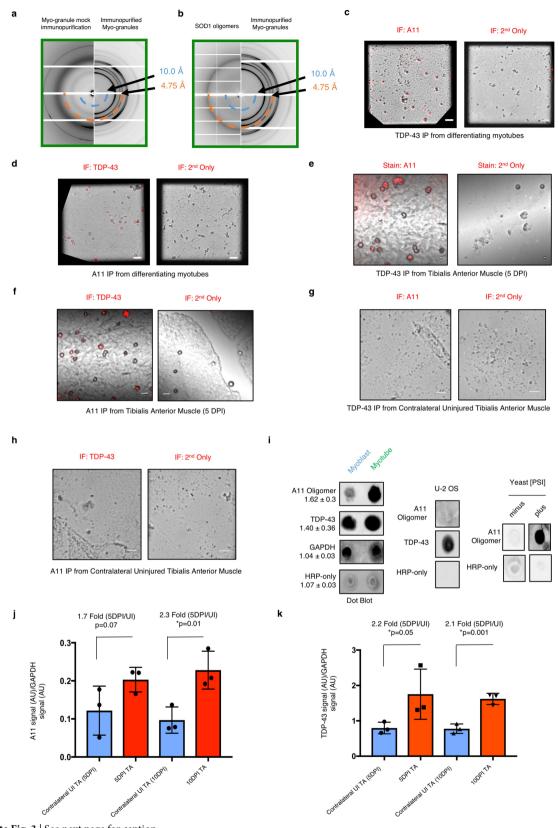
Extended Data Fig. 1 | See next page for caption.

Extended Data Fig. 1 | Increased cytosolic TDP-43 during normal skeletal muscle formation. Related to Fig. 1. **a**, Nuclear localization of TDP-43 immunofluorescence in C2C12 myoblasts and both nuclear and cytoplasmic localization in C2C12 myotubes differentiated for seven days ($n = 3$ independent experiment). Myosin heavy chain (MHC) identifies differentiated cells. Scale bars, 25 μm. **b**, Subcellular fractionation reveals increased cytosolic TDP-43 in differentiating myotubes. Cytosolic (Cyto) myoblasts, $5.0 \pm 2.1\%$; cytosolic myotubes, $19.7 \pm 3.1\%$; $n = 3$ biologically independent experiments that showed similar results, unpaired, two-tailed Student's t-test, $P = 2.0 \times 10^{-3}$. **c**, Time course of TDP-43 expression during skeletal-muscle differentiation. $n = 3$ independent experiments with similar results. Myogenin (MyoG) (magenta) and MHC (green) identify differentiated cells. Nuclei were counterstained with DAPI. Scale bars, 25 μm. **d**, Top, TDP-43 expression in primary myotubes derived from muscle stem cells that were differentiated in culture for four days. $n = 3$ independent experiments with similar results. Bottom, images for a secondary-antibody only control. Scale bars, 25 μm. **e**, Deconvolution microscopy of TDP-43 expression in C2C12 myotubes differentiated for five days. Scale bar, 5 μm. $n = 3$ independent experiments with similar results. **f**, CRISPR–Cas9-mediated genomic integration of tetracycline-inducible HaloTag–TDP-43 into the *Rosa26* safe-harbour locus in C2C12 myoblasts. A, B and C represent approximate location of primers used in **g**. **g**, PCR analyses of gDNA from C2C12 myoblasts for the presence of the HaloTag–TDP-43 construct (top) and integration of the construct into the *Rosa26* locus (bottom) using the primers shown in **f**. $n = 3$ independent experiments with similar results. Red arrowheads point to the expected PCR product for integration of HaloTag–TDP-43 into *Rosa26*. Subsequent live-imaging experiments were performed using clones 1 and 4. Non-specific bands are indicated by an asterisk. **h**, Detection of fluorescently labelled HaloTag–TDP-43 in C2C12 myoblasts following induction resolved on SDS–PAGE. Janelia Fluor 646 (JF646). $n = 3$ independent experiments with similar results. **i**, Detection of both HaloTag–TDP-43 and endogenous TDP-43 in selected C2C12 cell clones. $n = 3$ independent experiments with similar results. **j, k**, Representative images of individual HaloTag–TDP-43 molecules in a myoblast (**j**) and a multinucleated myotube (**k**). Top, start of acquisition (frame 1). Nuclei (Nuc) and cytosolic borders are demarcated by white dotted lines. $n = 3$ independent experiments with similar results. Bottom, dynamic mapping of single TDP-43 molecule tracks using a multiple target tracing MATLAB script[46]. Vibrant violet was used to detect myonuclei. Scale bars, 5 μm.

Extended Data Fig. 2 | During muscle formation TDP-43 adopts a higher-order state distinct from stress granules. Related to Fig. 1. **a**, Secondary antibody-only control for TDP-43 staining of tibialis anterior muscle sections at 5 DPI. Scale bar, 25 μm. $n = 5$ mice per condition, representative images are shown, all experiments showed similar results. Nuclei were counterstained with DAPI. **b**, Representative images of TDP-43 and eMHC immunostaining in tibialis anterior muscle sections at 30 DPI; nuclei were counterstained with DAPI. $n = 4$ mice. Scale bar, 50 μm. **c**, RIPA–urea assay reveals the presence of an urea-insoluble TDP-43 fraction isolated from C2C12 myotubes that were differentiated for seven days, but not in C2C12 myoblasts. $n = 3$ independent experiments, each showing similar results, unpaired, two-tailed Student's t-test, $P = 0.0008$. GAPDH remains RIPA-soluble in both myoblasts and myotubes. $n = 3$ independent experiments, each showing similar results, unpaired, two-tailed Student's t-test, $P = 0.7443$. **d**, Higher molecular
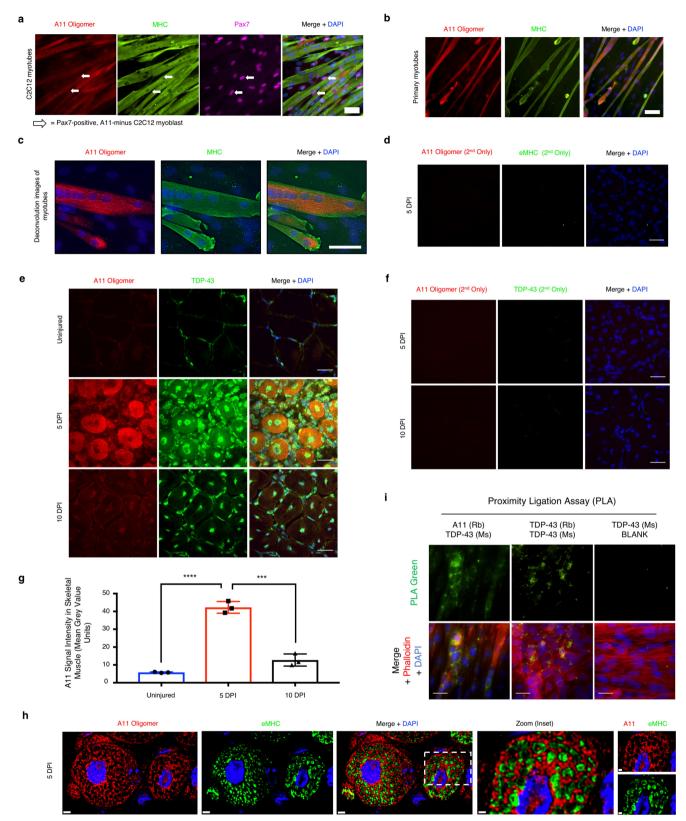
weight SDS-resistant TDP-43 assemblies were present in differentiating C2C12 myotubes. Protein assemblies resolved by SDD–AGE. $n = 3$ independent experiments. Pub1Q/N-GFP from yeast forms SDS-resistant assemblies that have a higher molecular weight than TDP-43 assemblies. **e**, Schematic of the isolation of myo-granules that contain TDP-43 that are formed during skeletal muscle formation. **f**, Immunoprecipitation (IP) of TDP-43 on Dynabeads (DB) reveals that oligomers isolated from C2C12 myotubes are absent from myoblasts as observed by TEM. $n = 3$ independent experiments. **g**, Stress-granule formation in multinucleated myotubes derived from C2C12 cells. Immunofluorescence using antibodies against stress-granule proteins, G3BP1 and PABP1, after NaAsO$_2$ treatment or control conditions for 60 min. $n = 3$ independent experiments, each showing similar results. Zoom, boxed area shown at higher magnification. Scale bars, 5 μm and 20 μm (insets).

Extended Data Fig. 3 | See next page for caption.

Extended Data Fig. 3 | Myo-granules isolated from cells and mice contain TDP-43 and are amyloid-like oligomers. Related to Fig. 2. **a**, **b**, X-ray diffraction of immunoprecipitated myo-granules (right half of **a**, **b**) compared to the diffraction of mock IgG immunoprecipitation (left half **a**) and to the diffraction of super oxide dismutase 1 (SOD1) amyloid oligomers (left half of **b**). For all diffraction patterns, two rings at approximately 4.8 Å and approximately 10 Å are drawn on the bottom half to highlight the absence of an approximately 4.8 Å reflection in the mock immunoprecipitation and a similar approximately 4.8 Å reflection with the absence of an approximately 10 Å reflection in the SOD1 diffraction. One sample per condition was used. Two diffraction images at different rotations were taken per sample and each image gave similar results. **c**, **d**, Complexes that were immunopurified using TDP-43 (**c**) or A11 (**d**) were isolated from C2C12 myotubes. Complexes express A11 (**c**) and TDP-43 (**d**), whereas immunopurified TDP-43 or A11 myo-granules that were immunostained with secondary antibodies only lack signal. Red, TDP-43 or A11 immunoreactivity. $n = 3$ independent experiments. Scale bars, 1 μm. **e**, **f**, Complexes that were immunopurified using TDP-43 (**e**) or A11 (**f**) were isolated from tibialis anterior muscle at 5 DPI.
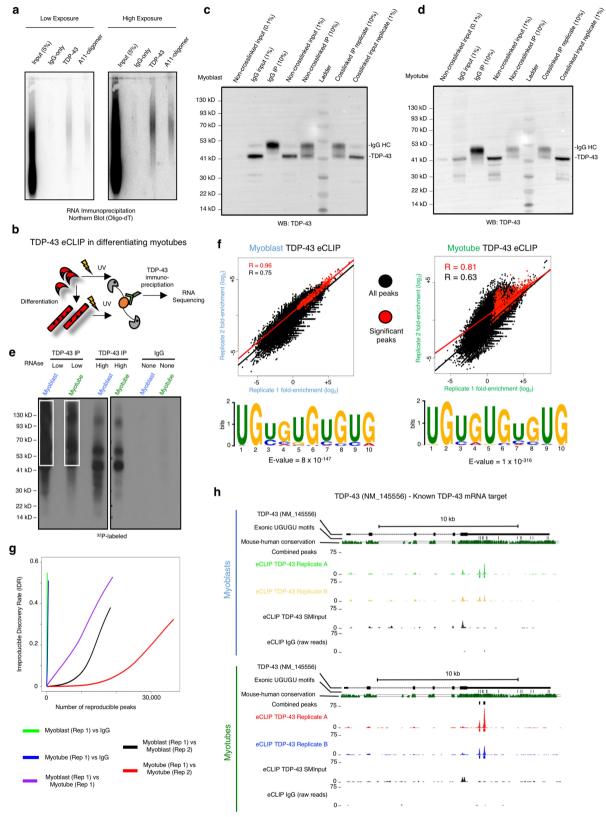
Complexes express A11 (**e**) and TDP-43 (**f**), whereas immunopurified TDP-43 or A11 myo-granules immunostained with secondary antibodies only lack signal. Red, TDP-43 or A11 immunoreactivity. $n = 3$ mice. Scale bars, 0.05 μm. **g**, TDP-43 immunopurified complexes isolated from an uninjured tibialis anterior muscle (contralateral to the 5 DPI muscle) reveal no complexes with an A11 oligomeric confirmation. $n = 3$ mice. Scale bars, 0.05 μm. **h**, A11 immunopurified complexes from an uninjured tibialis anterior muscle (contralateral to the 5 DPI muscle) reveal no complexes containing TDP-43. $n = 3$ mice. Scale bars, 0.05 μm. **i**, Dot blot of A11 immunoreactivity in C2C12 cells differentiated into myotubes compared to myoblasts. Quantification reflects fold change in dot blot signal from myoblast to myotube. Data are mean ± s.d., $n = 3$ independent experiments. **j**, **k**, Quantification of the dot blot signal for A11 conformation complexes (**j**) and TDP-43 conformation complexes (**k**) during skeletal muscle regeneration at 5 DPI and 10 DPI compared to contralateral uninjured tibialis anterior muscle and normalized to the HRP-only signal. Quantification reflects fold change in dot blot signal. Data are mean ± s.d., $n = 3$ mice, P values were obtained using unpaired, two-tailed Student's t-tests.

= Pax7-positive, A11-minus C2C12 myoblast

Extended Data Fig. 4 | See next page for caption.

Extended Data Fig. 4 | Myo-granules in skeletal muscle contain TDP-43 and are amyloid-like oligomers. Related to Fig. 2. **a**, C2C12 myotubes differentiated for seven days reveal strong A11 immunoreactivity in MHC$^+$ myotubes, but no A11 immunoreactivity in undifferentiated PAX7$^+$ myoblasts. $n = 3$ independent experiments. Scale bar, 50 μm. **b**, Muscle stem cells isolated from four-month-old C57/BL6 mice were differentiated in culture for five days and show cytoplasmic and nuclear expression of A11 oligomers. Myotubes express MHC. Scale bar, 50 μm. $n = 3$ mice. **c**, Deconvolution microscopy of C2C12 myotubes differentiated for seven days reveal punctate A11 staining in MHC$^+$ myotubes, but no A11 signal was found in undifferentiated myoblasts. Scale bar, 25 μm. $n = 3$ independent experiments. **d**, Secondary antibody-only control for A11 staining in tibialis anterior muscle sections at 5 DPI. Nuclei were counterstained with DAPI. Scale bar, 25 μm. $n = 4$ mice. **e**, Representative images of A11 and TDP-43 co-localization in tibialis anterior muscle for uninjured muscles, and at 5 DPI and 10 DPI. Scale bars, 25 μm. $n = 3$ mice. **f**, Secondary antibody-only control for A11–TDP-43 co-localization in tibialis anterior muscle sections at 5 DPI and 10 DPI shows a lack of signal. Nuclei were counterstained with DAPI. Scale bar, 25 μm. $n = 3$ mice. **g**, Quantification of A11 signal intensity in myofibres from **e**. Unpaired, two-tailed Student's t-test; comparison between uninjured muscle and 5 DPI, ****$P = 4.4 \times 10^{-5}$; comparison between 5 DPI and 10 DPI, ***$P = 4.1 \times 10^{-4}$; comparison between 10 DPI and uninjured muscle $P = 0.024$ (P value not shown). $n = 3$ mice per condition, $n = 10$ myofibres were averaged per mouse. Data are mean ± s.d. **h**, Representative deconvolution image of A11 immunoreactivity and eMHC expression in the mouse tibialis anterior myofibres at 5 DPI that were quantified in Fig. 2c. $n = 3$ mice, each showing similar results. Scale bars, 2 μm and 0.8 μm (inset). **i**, Proximity ligation assays reveal complexes of TDP-43 and A11 (green) in C2C12 myotubes counterstained with phalloidin (red). A PLA positive control with two antibodies that recognize different epitopes of TDP-43 are positive, whereas complexes are absent if one primary antibody is omitted. $n = 3$ independent experiments per condition. Ms, mouse; Rb, rabbit.
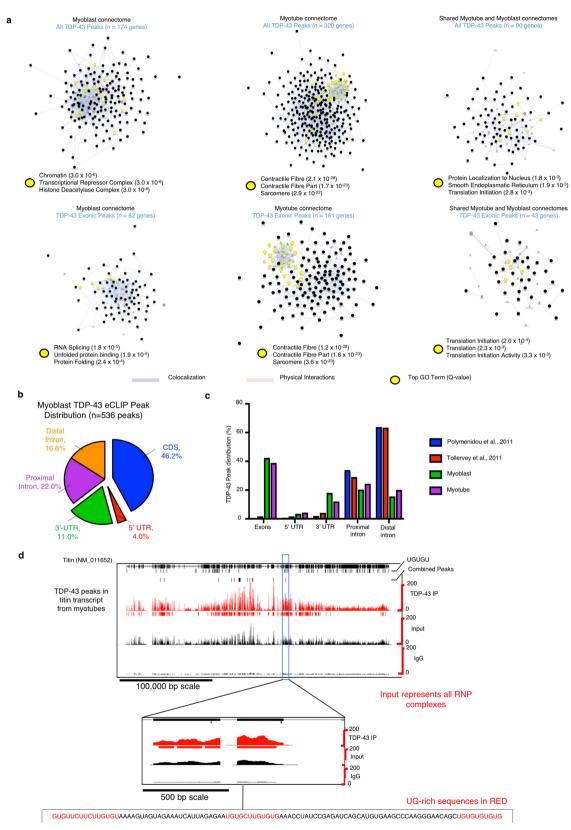
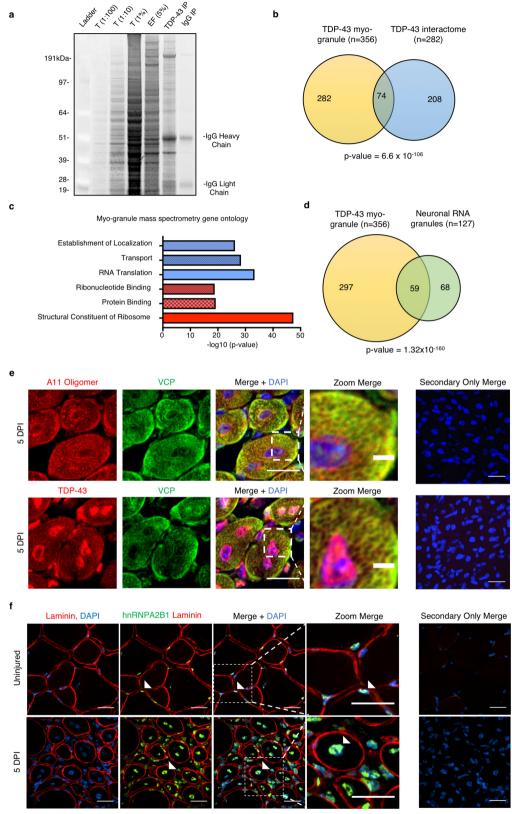**Extended Data Fig. 5 |** See next page for caption.

Extended Data Fig. 5 | TDP-43 eCLIP on skeletal muscle myoblasts and myotubes. Related to Fig. 3. **a**, RNA immunoprecipitation of C2C12 myotubes, followed by oligo-dT northern blot. Analyses reveal that A11 and TDP-43 associate with poly-A RNA. $n = 3$ biologically independent samples. **b**, Schematic of the eCLIP protocol for cultured C2C12 myoblasts and myotubes. **c**, Immunoprecipitation of TDP-43 complexes used for eCLIP in C2C12 myoblasts. $n = 2$ biologically independent samples. **d**, Same as in **c**, but for C2C12 myotubes. $n = 2$ biologically independent samples. **e**, Autoradiogram of ^{32}P-labelled TDP-43–RNA complexes fractionated by PAGE. White boxes indicate the area cut and used for eCLIP library preparation. $n = 1$ library was prepared per condition. **f**, Top, scatter plots indicate correlation between significant TDP-43 eCLIP peaks in biological replicates. Scatter plots represent fold enrichment for each region in TDP-43 eCLIP relative to paired size-matched input with significant peaks in red ($P \leq 10^{-8}$ over size-matched input). P values for each peak to determine significance were calculated by Yates' χ^2 test (Perl), or Fisher exact test (R computing software) when the expected or observed read number was below five[16]. For myoblasts, R values were calculated using $n = 511,137$ non-significant peaks and $n = 596$ significant peaks. For myotubes, R values were calculated using $n = 413,368$ non-significant peaks and $n = 1,501$ significant peaks. Bottom, the UG-rich motif is significantly enriched in clusters from open reading frames and untranslated regions (UTRs). E values were determined using the DREME software tool. **g**, Irreproducible discovery rate analysis comparing peak fold enrichment across indicated datasets. **h**, TDP-43 eCLIP reveals that TDP-43 binds to the 3′ UTR of the TDP-43 transcript in myoblasts (top) and myotubes (bottom). $n = 3$ biologically independent experiments, each showing similar results.

Extended Data Fig. 6 | TDP-43 binds to mRNAs that encode sarcomeric proteins during muscle formation. Related to Fig. 3. **a**, Myoblast (left), myotube (middle) and shared (right) connectome analysis for all TDP-43 eCLIP peaks (top) and TDP-43 exonic peaks (bottom). **b**, TDP-43 binds predominantly to exons of protein-coding RNAs in C2C12 myoblasts. **c**, Peak distribution for significantly enriched TDP-43 peak locations in myoblasts and 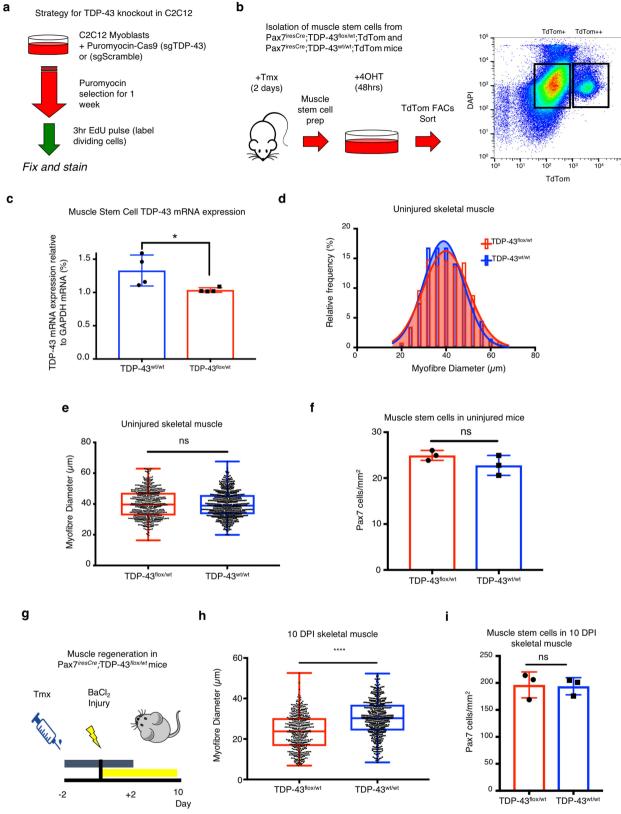myotubes across the transcriptome reveal increased exonic and 3′-UTR associations compared to previously identified neuronal TDP-43 peaks[18,19]. **d**, Identification of multiple TDP-43-binding sites across and within exons of *Ttn*. The zoomed region is representative of multiple UG-rich sequences within a single exon. $n = 3$ biologically independent experiments, each showing similar results.

a

b

TDP-43 myo-granule (n=356)   TDP-43 interactome (n=282)

282   74   208

p-value = 6.6×10^{-106}

c

Myo-granule mass spectrometry gene ontology

Establishment of Localization
Transport
RNA Translation
Ribonucleotide Binding
Protein Binding
Structural Constituent of Ribosome

-log10 (p-value)

d

TDP-43 myo-granule (n=356)   Neuronal RNA granules (n=127)

297   59   68

p-value = 1.32×10^{-160}

e

A11 Oligomer | VCP | Merge + DAPI | Zoom Merge | Secondary Only Merge

5 DPI

TDP-43 | VCP | Merge + DAPI | Zoom Merge

5 DPI

f

Laminin, DAPI | hnRNPA2B1 Laminin | Merge + DAPI | Zoom Merge | Secondary Only Merge

Uninjured
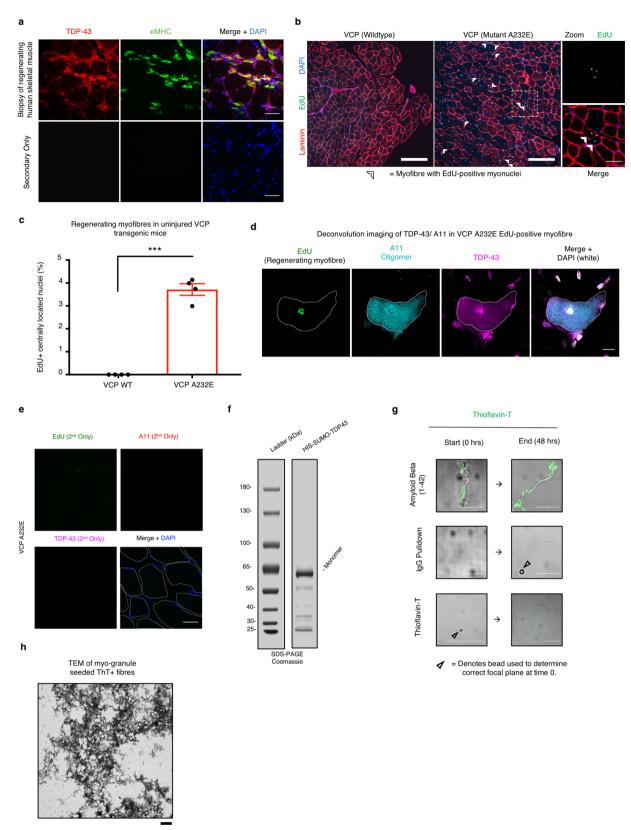
5 DPI

Extended Data Fig. 7 | See next page for caption.

Extended Data Fig. 7 | Myo-granule protein composition. Related to Fig. 3. **a**, SDS–PAGE gel stained with SYPRO Ruby reveals enrichment of select proteins during fractionation of total cell lysate (T) from C2C12 myotubes, the enriched fraction (EF) and immunoprecipitation of TDP-43. $n = 3$ biologically independent experiments, each showing similar results. TDP-43 and IgG control immunoprecipitation experiments are representative of the fractions used for mass spectrometry. **b**, Venn diagram showing significant overlap between the myo-granule proteome and TDP-43 interactome (previously defined[22]). The P value was determined using a hypergeometric test. **c**, Gene Ontology of myo-granules reveals enrichment for processes relating to the localization and translation of RNA. $n = 356$ proteins, P values were determined using hypergeometric tests with Benjamini–Hochberg false-discovery rate corrections. **d**, Venn diagram showing significant overlap between myo-granules and neuronal RNA granule proteomes (previously defined[23]). P value was determined using a hypergeometric test. **e**, VCP, a top hit in the myo-granule proteome, co-localizes with the cytoplasmic TDP-43 and A11 signals in mouse skeletal muscle at 5 DPI. $n = 3$ mice. **f**, The RNA-binding protein HNRNPA2B1 is not associated with the myo-granule proteome and remains localized in myonuclei in injured (5 DPI) and uninjured tibialis anterior muscle. $n = 3$ mice.

a Strategy for TDP-43 knockout in C2C12

b Isolation of muscle stem cells from Pax7^{iresCre};TDP-43$^{flox/wt}$;TdTom and Pax7^{iresCre};TDP-43$^{wt/wt}$;TdTom mice

c Muscle Stem Cell TDP-43 mRNA expression

d Uninjured skeletal muscle

e Uninjured skeletal muscle

f Muscle stem cells in uninjured mice

g Muscle regeneration in Pax7^{iresCre};TDP-43$^{flox/wt}$ mice

h 10 DPI skeletal muscle

i Muscle stem cells in 10 DPI skeletal muscle

Extended Data Fig. 8 | See next page for caption.

Extended Data Fig. 8 | TDP-43 is an essential protein for skeletal muscle formation. Related to Fig. 3. **a**, Schematic of the approach used to knockout *Tardbp* and quantify C2C12 myoblast proliferation. **b**, Schematic of the isolation and fluorescence-activated cell sorting (FACS) of muscle stem cells from $Pax7^{IREScre}Tardbp^{flox/WT}Rosa26^{tdTomato}$ and $Pax7^{IREScre}Tardbp^{WT/WT}Rosa26^{tdTomato}$ mice. More than 125,000 muscle stem cells were collected per mouse from two populations defined in **b** as TdTom$^+$ and TdTom^{++}. **c**, *Tardbp* mRNA expression relative to *Gapdh* mRNA expression from isolated muscle stem cells from **b**. $n = 4$ independent experiments, each a mean of technical triplicates, from $n = 2$ mice. Unpaired, two-tailed Student's *t*-test, *$P = 0.0469$. Data are mean ± s.d. **d**, Myofibre feret diameter frequency distribution in uninjured $Pax7^{IREScre}Tardbp^{flox/WT}$ mice compared to $Pax7^{IREScre}Tardbp^{WT/WT}$ controls. $n = 3$ mice, 600 myofibres were quantified per condition. **e**, Quantification of myofibre feret diameter shown in **c**. In the box plots, the horizontal bars show the mean, boxes show the 25th and 75th percentiles, whiskers show the minimum and maximum, individual

myofibres are shown as dots. $n = 3$ mice, 600 myofibres per condition. Unpaired, two-tailed Student's *t*-test, P $= 0.5925$; ns, not significant. **f**, Pax7$^+$ muscle stem cell numbers in uninjured $Pax7^{IREScre}Tardbp^{flox/WT}$ mice compared to $Pax7^{IREScre}Tardbp^{WT/WT}$ controls. $n = 3$ mice. Unpaired, two-tailed Student's *t*-test, $P = 0.1963$. Data are mean ± s.d. **g**, Schematic of TDP-43 depletion in Pax7$^+$ muscle stem cells during muscle regeneration in $Pax7^{IREScre}Tardbp^{flox/WT}$ and $Pax7^{IREScre}Tardbp^{WT/WT}$ mice. Tmx, tamoxifen. **h**, Quantification of myofibre feret diameters from Fig. 3h at 10 DPI in muscle stem cells from $Pax7^{IREScre}Tardbp^{flox/WT}$ mice compared to wild-type controls. In the box plots, the horizontal bars show the mean, boxes show the 25th and 75th percentiles, whiskers show the minimum and maximum, individual myofibres are shown as dots. $n = 489$ myofibres from $n = 3$ mice per condition. Unpaired, two-tailed Student's *t*-test, ****$P = 2.3 \times 10^{-30}$. **i**, Similar Pax7$^+$ muscle stem cell numbers at 10 DPI in muscle stem cells from $Pax7^{IREScre}Tardbp^{flox/WT}$ haploinsufficient mice compared to wild-type controls. Data are mean ± s.d. from $n = 3$ mice. Unpaired, two-tailed Student's *t*-test, $P = 0.89$.

a

Biopsy of regenerating human skeletal muscle

TDP-43 eMHC Merge + DAPI

Secondary Only

b

VCP (Wildtype) VCP (Mutant A232E) Zoom EdU

DAPI EdU Laminin

⊾ = Myofibre with EdU-positive myonuclei

Merge

c

Regenerating myofibres in uninjured VCP transgenic mice

***

EdU+ centrally located nuclei (%)

VCP WT VCP A232E

d

Deconvolution imaging of TDP-43/ A11 in VCP A232E EdU-positive myofibre

EdU (Regenerating myofibre) A11 Oligomer TDP-43 Merge + DAPI (white)

e

VCP A232E

EdU (2nd Only) A11 (2nd Only)

TDP-43 (2nd Only) Merge + DAPI

f

Ladder (kDa) HIS-SUMO-TDP43

180-
130-
100-
65- - Monomer
50-
40-
30-
25-

SDS-PAGE Coomassie

g

Thioflavin-T

Start (0 hrs) End (48 hrs)

Amyloid Beta (1-42) →

IgG Pulldown →

Thioflavin-T →

◁ = Denotes bead used to determine correct focal plane at time 0.

h

TEM of myo-granule seeded ThT+ fibres

Extended Data Fig. 9 | See next page for caption.

Extended Data Fig. 9 | Myo-granules that seed amyloid-like fibres are increased in human muscle regeneration and in multisystem proteinopathy. Related to Figs. 4, 5. **a**, Representative images of TDP-43 expression (top) and secondary antibody-only control (bottom) in regenerating human skeletal muscle from a patient with necrotizing myopathy. $n = 3$ independent patient biopsies, each showing similar results. Scale bars, 50 μm. **b**, Representative tibialis anterior cross-section images of uninjured VCP(A232E) and VCP(WT) mice labelled with EdU after 21 days of EdU treatment in the drinking water to mark division and fusion of muscle stem cells. Laminin identifies myofibres and cells are stained with DAPI to identify nuclei. Arrowheads indicate myofibres with EdU$^+$ centrally located myonuclei. $n = 3$ mice, each showing similar results. Scale bars, 200 μm and 50 μm (inset). **c**, Quantification of myofibres with EdU$^+$ centrally located myonuclei in VCP(A232E) and VCP(WT) mice. $n = 4$ mice, over 1,000 myofibres were quantified per genotype. Data are mean ± s.d. Unpaired, two-tailed Student's t-test,

$P = 6.5 \times 10^{-6}$. **d**, Representative deconvolution image of A11 and TDP-43 co-localization in a regenerating myofibre from a VCP(A232E) tibialis anterior muscle. $n = 3$ mice, each showing similar results. Scale bar, 10 μm. **e**, Secondary antibody-only control of uninjured VCP(A232E) tibialis anterior muscle sections reveals a lack of signal. Nuclei were counterstained with DAPI and myofibres were outlined in white. $n = 4$ mice, each showing similar results. Scale bar, 25 μm. **f**, Coomassie-stained recombinant HIS–SUMO–TDP-43 used for thioflavin-T assays resolved by SDS–PAGE. $n = 3$ biologically independent experiments, each showing similar results. **g**, Thioflavin-T incorporation reveals thioflavin-T$^+$ amyloid-like fibres for recombinant amyloid-β_{1-42} and absence of thioflavin-T signal in both the IgG pull-down control and thioflavin-T alone. $n = 3$ biologically independent experiments, each showing similar results. Scale bars, 10 μm. **h**, Representative TEM image (zoomed out from Fig. 5e) of thioflavin-T$^+$ (ThT) fibres formed from isolated myo-granules. $n = 3$ biologically independent experiments. Scale bar, 1 μm.

Extended Data Fig. 10 | Myo-granules in normal skeletal muscle regeneration and in disease. Schematic of TDP-43 oligomerization and aggregation in wild-type, ageing and diseased skeletal muscle myofibres.

nature research

Corresponding author(s):   Roy Parker, Bradley B. Olwin

Reporting Summary

Nature Research wishes to improve the reproducibility of the work that we publish. This form provides structure for consistency and transparency in reporting. For further information on Nature Research policies, see Authors & Referees and the Editorial Policy Checklist.

Statistical parameters

When statistical analyses are reported, confirm that the following items are present in the relevant location (e.g. figure legend, table legend, main text, or Methods section).

n/a	Confirmed	
☐	☒	The exact sample size (n) for each experimental group/condition, given as a discrete number and unit of measurement
☐	☒	An indication of whether measurements were taken from distinct samples or whether the same sample was measured repeatedly
☐	☒	The statistical test(s) used AND whether they are one- or two-sided *Only common tests should be described solely by name; describe more complex techniques in the Methods section.*
☐	☒	A description of all covariates tested
☒	☐	A description of any assumptions or corrections, such as tests of normality and adjustment for multiple comparisons
☐	☒	A full description of the statistics including central tendency (e.g. means) or other basic estimates (e.g. regression coefficient) AND variation (e.g. standard deviation) or associated estimates of uncertainty (e.g. confidence intervals)
☐	☒	For null hypothesis testing, the test statistic (e.g. F, t, r) with confidence intervals, effect sizes, degrees of freedom and P value noted *Give P values as exact values whenever suitable.*
☒	☐	For Bayesian analysis, information on the choice of priors and Markov chain Monte Carlo settings
☒	☐	For hierarchical and complex designs, identification of the appropriate level for tests and full reporting of outcomes
☒	☐	Estimates of effect sizes (e.g. Cohen's d, Pearson's r), indicating how they were calculated
☐	☒	Clearly defined error bars *State explicitly what error bars represent (e.g. SD, SE, CI)*

Our web collection on statistics for biologists may be useful.

Software and code

Policy information about availability of computer code

Data collection	DeltaVision softWoRx 6.5.2 Software Suite, Nikon Elements Viewer 4.11.0
Data analysis	ImageJ: v. 2.0.0-rc-43/1.52e, Cutadapt: v. 1.11, STAR: v. STAR_2.5.1b, Samtools: v. 1.5, bedToBigBed: v. 2.7, Bedtools: v.2.26.0, R: v. 3.2.3, clipper 0.2.0, Python 2.7.8, eCLIP pipeline scripts downloaded from https://github.com/gpratt/gatk/releases/tag/2.3.2. IDR R scripts downloaded from https://sites.google.com/site/anshulkundaje/projects/idr. UCSC genome browser. Microsoft Excel: v. 16.16 (180812). Imaris x64: v 9.2.1., MaxQuant/Andromeda(v 1.5.0.12

For manuscripts utilizing custom algorithms or software that are central to the research but not yet described in published literature, software must be made available to editors/reviewers upon request. We strongly encourage code deposition in a community repository (e.g. GitHub). See the Nature Research guidelines for submitting code & software for further information.

Data

Enhanced CLIP data is available on GEO (https://www.ncbi.nlm.nih.gov/geo/query/acc.cgi?acc=GSE104796) under accession number GEO: GSE104796. Source data are provided for Fig. 1d, 2c, 3f, 3h, 4c, 5b, 5c and Extended Data Fig. 1b, 2c, 3i-k, 4g, 7c, 7f, 7h, 7i, 8c and 9c. All other data supporting the findings of this study are available within the article supplemental materials. Data are available upon request from the corresponding authors.

Field-specific reporting

Please select the best fit for your research. If you are not sure, read the appropriate sections before making your selection.

☒ Life sciences ☐ Behavioural & social sciences ☐ Ecological, evolutionary & environmental sciences

For a reference copy of the document with all sections, see nature.com/authors/policies/ReportingSummary-flat.pdf

Life sciences study design

All studies must disclose on these points even when the disclosure is negative.

Sample size	Samples sizes (n=3, unless otherwise stated) were chosen according to field standards.
Data exclusions	No data was excluded.
Replication	All replication attempts were successful. Multiple authors independently replicated the TDP-43 localization and A11 localization studies in mice cell culture (T.O.V., O.N.W., and J.R.W.). Multiple authors in different labs replicated myo-granule identification in human samples (T.O.V. and K.A.B.). eCLIP studies were replicated as described in Extended Data Fig 5f. All myo-granule isolation attempts were successful and detailed in the methods with citations to published methods.
Randomization	Experimental mice were randomly assigned using age-matched, sex-matched controls. In mouse experiments where genotypes were assigned age-matched, sex-matched mice were used to control for co-variables. Experiments performed in cell lines were assigned randomly against wild type conditions or against scramble controls were necessary. Biochemical experiments were assigned randomly against both positive controls (were applicable) and with negative controls to assess background and specificity.
Blinding	Authors were blinded to the clinical and pathological diagnosis of human samples. Otherwise no blinding was used.

Reporting for specific materials, systems and methods

Materials & experimental systems

n/a	Involved in the study
☒	☐ Unique biological materials
☐	☒ Antibodies
☐	☒ Eukaryotic cell lines
☒	☐ Palaeontology
☐	☒ Animals and other organisms
☐	☒ Human research participants

Methods

n/a	Involved in the study
☒	☐ ChIP-seq
☐	☒ Flow cytometry
☒	☐ MRI-based neuroimaging

Antibodies

Antibodies used	Primary Antibodies 1. Monoclonal mouse anti-Pax7 (DSHB, Developmental Studies Hybridoma Bank, AB-528428, Clone: Pax7) was used for immunofluorescence (IF) at 1:750 for staining tissue sections and cells. 2. Polyclonal rabbit anti-Laminin (Sigma-Aldrich, L9393) was used for IF at 1:200 for staining tissue sections. Lot# 015M4881V 3. Polyclonal rabbit anti-TDP-43 (N-terminal) (Proteintech, 10782-2-AP) was used for IF at 1:200 or 1:400 for staining tissue

sections and cells, for western blot (WB) at 1:1000, for dot blot (DB) at 1:1000, for immunoprecipitation (IP) at 1 μg/uL, for correlative light electron microscopy (CLEM) at 1:100. Antigen Catalog #: Ag1231
4. Polyclonal rabbit anti-TDP-43 (C-terminal) (Proteintech, 12892-1-AP) was used for IF at 1:200 or 1:400 for staining tissue sections and cells and for correlative light electron microscopy (CLEM) at 1:100. Antigen listed on manufacturer's website.
5. Monoclonal mouse anti-TDP-43 (Abcam, ab57105) was used for IF at 1:200 for staining tissue sections and cells. Clone 2E2-D3, Lot# GR303763-9.
6. Polyclonal rabbit anti-TDP-43 (Bethyl Laboratories, A303-223A) Lot#: 1. 5 μg was used for IP and for WB at 1:2000.
7. Polyclonal rabbit anti-Anti Oligomer (A11) antibodies were obtained from Charles Glabe as noted in acknowledgments (A11 polyclonal sera lot 40mg). A11 was used for IF at 1:200 or 1:400 for staining tissue sections and cells, for DB at 1:1000, for IP at 1 μg/uL, forCLEM at 1:100.
8. Monoclonal mouse anti-Myosin (eMHC, Clone: F1.652) (DSHB, Developmental Studies Hybridoma Bank, AB_528358) was used for immunofluorescence (IF) at 1:5 for staining tissue sections and cells.
9. Monoclonal mouse anti-Myosin (MHC, Clone: MF20) (DSHB, Developmental Studies Hybridoma Bank, AB_2147781) was used for immunofluorescence (IF) at 1:1 for staining tissue sections and cells.
10. Monoclonal mouse anti-GFP (Covance, MMS-118P. Clone B34) was used for WB at 1:1000.
11. Monoclonal rabbit anti-GAPDH (14C10) conjugated to HRP (horseradish peroxidase) (Cell Signaling, 3683S) was used for WB at 1:2000.
12. Monoclonal mouse anti-VCP (Thermo, MA3-004. Lot# SC247485) was used for IHC at 1:400.

Secondary Antibodies
1. Anti-Rabbit IgG HRP (Cell Signaling, 7074S) was used for WB at 1:10000.
2. Anti-Mouse IgG HRP (Cell Signaling, 7076S) was used for WB at 1:10000.
3. Anti-Rabbit IgG Alexa Fluor 647 (Abcam, ab150079) was used for staining CLEM samples at 1:250.
4. Anti-Rabbit IgG Alexa Fluor 647 (Thermo Scientific, A-31573) was used for staining cells and tissue sections at 1:1000.
5. Anti-Rabbit IgG Alexa Fluor 555 (Thermo Scientific, A-31572) was used for staining cells and tissue sections at 1:1000.
6. Anti-Mouse IgG1(gamma1) Alexa Fluor 647 (Thermo Scientific, A-21240) was used for staining cells and tissue sections at 1:1000.
7. Anti-Mouse IgG1(gamma1) Alexa Fluor 488 (Thermo Scientific, A-21121) was used for staining cells and tissue sections at 1:1000.
8. Anti-Mouse IgG2b-FITC (Southern Biotechnology Associates Inc., 1090-02) was used for staining cells and tissue sections at 1:1000

Validation

Primary Antibodies
1. Monoclonal mouse anti-Pax7 (DSHB, Developmental Studies Hybridoma Bank, AB-528428). Validation statements and relevant publications were provided by manufacture's website.
2. Polyclonal rabbit anti-Laminin (Sigma-Aldrich, L9393). Validation statements and relevant publications were provided by manufacture's website.
3. Polyclonal rabbit anti-TDP-43 (N-terminal) (Proteintech, 10782-2-AP). Validation statements and relevant publications were provided by manufacture's website.
4. Polyclonal rabbit anti-TDP-43 (C-terminal) (Proteintech, 12892-1-AP). Validation statements and relevant publications were provided by manufacture's website.
5. Monoclonal mouse anti-TDP-43 (Abcam, ab57105). Validation statements and relevant publications were provided by manufacture's website.
6. Polyclonal rabbit anti-TDP-43 (Bethyl Laboratories, A303-223A). Validation statements and relevant publications were provided by manufacture's website.
7. Polyclonal rabbit anti-Anti Oligomer (A11) antibodies were obtained from Charles Glabe as noted in acknowledgments (A11 polyclonal sera lot 40mg). Validation supported by citation Kayed et al. 2003.
8. Monoclonal mouse anti-Myosin (eMHC, F1.652) (DSHB, Developmental Studies Hybridoma Bank, AB_528358). Validation statements and relevant publications were provided by manufacture's website.
9. Monoclonal mouse anti-Myosin (MHC, MF20) (DSHB, Developmental Studies Hybridoma Bank, AB_2147781) Validation statements and relevant publications were provided by manufacture's website.
10. Monoclonal mouse anti-GFP (Covance, MMS-118P) was used for WB at 1:1000. Validation statements and relevant publications were provided by manufacture's website.
11. Monoclonal rabbit anti-GAPDH conjugated to HRP (horseradish peroxidase) (Cell Signaling, 3683S). Validation statements and relevant publications were provided by manufacture's website.
12. Monoclonal mouse anti-VCP (Thermo, MA3-004). Validation statements and relevant publications were provided by manufacture's website.

Eukaryotic cell lines

Policy information about cell lines

Cell line source(s)

Both C2C12 myoblasts and U-2 OS (human osteosarcoma) cells were purchased from ATCC (American Type Culture Collection).

Authentication

Authentication procedures for each cell line were performed according to industry standards of ATCC by microscopic cell morphology and growth rate analysis. For C2C12 cells, differentiation into and morphology of myotubes was used to authenticate cells.

Mycoplasma contamination

Cell lines tested negative for myoplasma.

Commonly misidentified lines
(See ICLAC register)

No commonly misidentified cell lines were used.

Animals and other organisms

Policy information about studies involving animals; ARRIVE guidelines recommended for reporting animal research

Laboratory animals	Mice were bred and housed according to National Institutes of Health (NIH) guidelines for the ethical treatment of animals in a pathogen-free facility at the University of Colorado at Boulder (Wild-type, Pax7iresCre, TDP-43flox/flox and VCP-A232E lines). The University of Colorado Institutional Animal Care and Use Committee (IACUC) approved animal protocols and procedures. Wild-type mice were C57Bl/6 (Jackson Labs, ME, USA) and VCP-A232E, VCPWT and TDP-43flox/flox mice were generated in a C57Bl/6 background as previously described (see methods). Crossing mice into Pax7iresCre mice generated conditional TDP-43flox/WT mice, also in the C57Bl/6 background. Cells and skeletal muscle tissue were isolated from 3-6-month-old male and female wild-type and Pax7iresCre; TDP-43flox/WT mice. Muscle tissue was isolated from 9-month-old male VCP-A232E mice. Control mice were age and sex matched from the mice and crosses described above.
Wild animals	None were used in this study.
Field-collected samples	None were used in this study.

Human research participants

Policy information about studies involving human research participants

Population characteristics	Under an IRB-approved protocol at Johns Hopkins University, a clinical muscle biopsy database was searched for patients who were clinically diagnosed with rhabodmyolysis and/or pathologically diagnosed with necrotizing myopathy with evidence of myofiber regeneration. Patient muscle tissue leftover from diagnostic biopsy was stored frozen at -80C for less than two years, and samples were cyrosectioned for immunohistochemical analysis.
Recruitment	No recruitment was performed for this study.

Flow Cytometry

Plots

Confirm that:

☒ The axis labels state the marker and fluorochrome used (e.g. CD4-FITC).

☒ The axis scales are clearly visible. Include numbers along axes only for bottom left plot of group (a 'group' is an analysis of identical markers).

☒ All plots are contour plots with outliers or pseudocolor plots.

☒ A numerical value for number of cells or percentage (with statistics) is provided.

Methodology

Sample preparation	Mass preparation for the isolation and expansions of muscle stem cells from the hindlimb skeletal muscle of Pax7iCre, TDP-43flox; TdTom+ mice.
Instrument	A MoFlo XDP Cell Sorter was used.
Software	FlowJo software was used for analysis.
Cell population abundance	>125,000 muscle stem cells expressing TdTom were isolate per mouse. These are the only relevant cells.
Gating strategy	Since these cells are genetically labeled we gated off the known TdTom florescence of mice without TdTom expression in muscle stem cells. Debris was excluded by FSC/SSC, doublets excluded by pulse width vs FSC area and collected cells were DAPI low and TdTom+ (as gated off negative control). DAPI-high positive cells were excluded as they represent dead cells.

☒ Tick this box to confirm that a figure exemplifying the gating strategy is provided in the Supplementary Information.